Master Thesis, Department of Geosciences

Diffractions and Their Multiples – Techniques to Enhance and Remove Them

By

Muhammad Umar

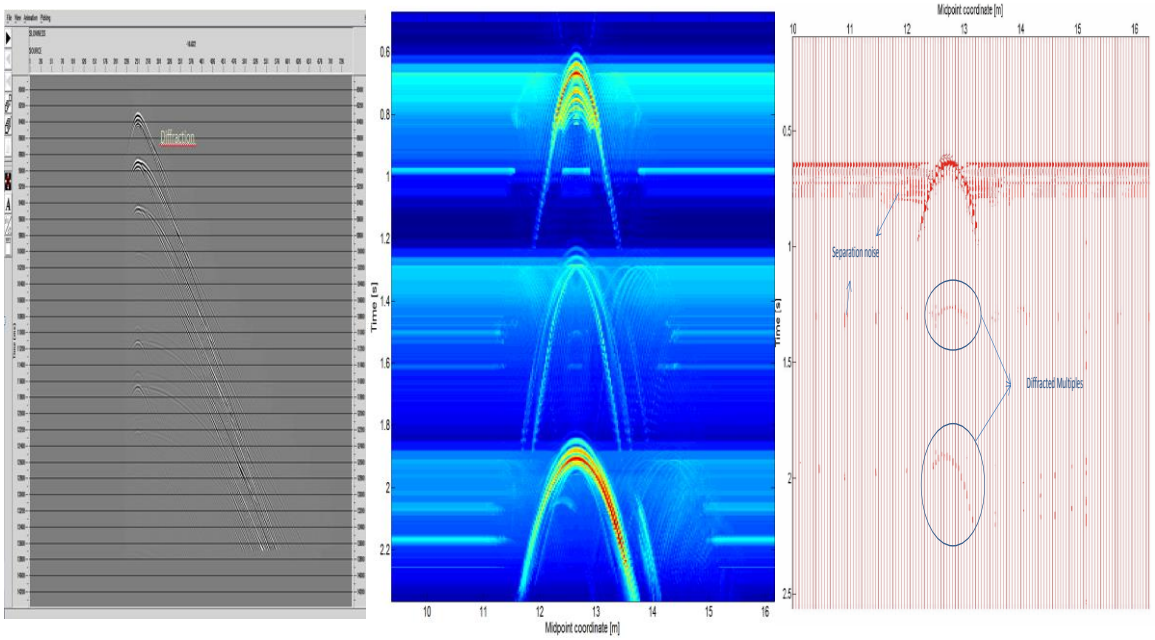

UNIVERSITY OF OSLO

FACULTY OF MATHEMATICS AND NATURAL SCIENCES

Diffractions and Their Multiples – Techniques to Enhance and Remove Them

By

Muhammad Umar

Master Thesis in Geosciences

Discipline: Geophysics

Department of Geosciences

Faculty of Mathematics and Natural Sciences

University of Oslo

June, 2014

Tutor(s): Professor Leiv-J. Gelius (UiO), Rune Øverås (PSS-Geo, Oslo)

This work is published digitally through DUO – Digitale Utgivelser ved UiO

http://www.duo.uio.no

It is also catalogued in BIBSYS (http://www.bibsys.no/english)

Acknowledgement

I feel instigated from within to extend my thanks to ALMIGHTY ALLAH (SWT) whose magnanimous and chivalrous blessings enabled me to perceive and pursue my ambitions and objectives. Special praises to Prophet Muhammad (PBUH), who is well wether for humanity as a whole.

I feel great honour in expressing my avid gratification to Professor Leiv-J. Gelius for his invaluable input and thought-provoking discussions during this present study. He has been tremendously supportive in shaping my thoughts to carry out this work within the time frame.

I also extend my special thanks to Jon Sandvik and Rune Øverås (PSS-Geo) for purposing this thesis. Special thanks to Rune Øverås for his guidance and professional support throughout my thesis.

I also express my special thanks to Endrias Getachew Asgedom for his esteemed suggestions and helping me throughout my work. Special thanks to my friends; especially CHILLAR GROUP from University of Oslo for providing me confidence and helps me in my education and other matters.

In the end my whole hearted and incessant gratitude to my loving parents, my brother, my sisters and wife, who always appreciated, encouraged and prayed for me.

P.S. ‘Please don’t restart this computer software is running’.

Muhammad Umar

01-06-2014

Abstract

The main focus of this thesis work has been diffractions and their associated multiples in marine seismic. Since diffraction carry useful information about small scale inhomogeneities in general, techniques able to enhance such events are of interest. By separating the weaker diffractions from reflections, such events can also be subtracted from the original data by adaptive techniques. Two different methods have been considered in this thesis: (i) plane wave destruction in the tau-p domain and (ii) modified Common Reflection Surface (CRS) technique. Both processing approaches have been tested employing both simple and more complex controlled data

TABLE OF CONTENTS

Chapter 1 MOTIVATION AND INTRODUCTION

In conventional seismic processing, reflected events are enhanced, but this information is in general not sufficient to image the small geological features such as faults and pinch-outs, wedges and reef edges etc (Faccipieri et al., 2013). However, seismic diffractions have been considered as an indicator for such geological features and small scale inhomogenities since they carry high resolution information (Landa and Keyder 1998; Khaidukov, Landa and Moser 2004). Thus, by enhancing the diffractions an image of high resolution can be obtained of the subsurface. This is the reason why diffraction enhancement is of interest. However, in some special cases, prediction followed by removal of diffracted energy will be equally important. Examples can be scattered energy caused by boulders on the seafloor or from ice in the water column. In case of a consolidated sea-floor, also associated water bottom multiples will be generated. This kind of scenario will be of main focus in this thesis.

In the last two decades different techniques have been proposed to separate diffractions from reflections. In the reflection focusing method (Khaidukov et al., 2004) diffractions are separated from reflections by muting reflections in the data leaving behind diffractions. Fomel, Landa and Taner (2007) used plane-wave destruction filters to suppress reflected events. Moser and Howard (2008) removed reflections by using anti-stationary filtering. Asgedom et al., (2011) used the modified Common Reflection Surface (CRS) technique to separate diffractions from reflections. This technique is also employed in this thesis to enhance the diffractions. Since the modified CRS technique does not predict amplitudes correctly, removal of diffractions using this procedure relies on a well-functioning adaptive subtraction method. This issue falls outside the scope of this thesis work. To subtract on eliminate contributions from diffractions (and possible multiples), we have therefore investigated the tau-p plane-wave destruction technique originally proposed by Taner and Fomel (2006).

The outline of this thesis is as follows. In chapter 2, we discuss the various types of noise with special emphasize on diffractions. In Chapter 3, we discuss the generation of synthetic

data sets (simple and complex) and further investigate different types of data sorting to unravel the behavior of diffractions and reflections. In Chapter 4, we explain plane-wave decomposition in the tau-p domain to eliminate diffractions and also introduce the modified version of CRS to enhance the diffractions. In Chapter 5, we discuss the results of both techniques for simple and complex synthetic data. Finally, Chapter 6 represents discussions and conclusions.

Chapter 2 NOISE

In general, seismic data consist of signal and noise. By definition we can say that any recorded signal which interferes with desired signal is considered as noise. Different types of noise usually contribute to the same data set. Therefore attenuation of noise is not straightforward due to these differences in noise characteristics. Thus, there is no simple procedure that can remove all noise from the seismic data during processing (Elboth et al., 2009b).

2.1 CLASSIFICATION OF NOISE

There are three main classes of seismic noise which will be described below. Then we will discuss in more details the noise present in the data used in this study.

2.1.1 NON-LINEAR COHERENT NOISE

Multiples and ghosts represent non-linear coherent noise (cf. Fig. 2.1). Water bottom multiples are defined as energy reflected many times between the sea bed and sea surface. The reflections from these two interfaces are considered to be strong due to the significant impedance contrasts (Gelius and Johansen, 2010)

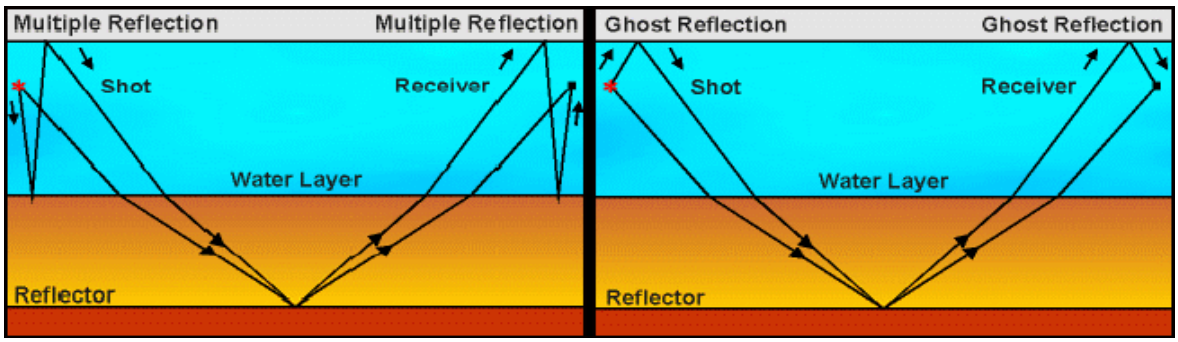

Figure2.1: Left: example of multiple reflections. Right: example of ghost reflections (Fugro Internal training notes, 2012).

Ghost reflections are considered as one of the most common forms of undesired seismic signals during marine acquisition. They represent reflections of up going direct energy from the sea surface. On the source side, these downward travelling waves will interfere with the direct downward travelling waves from the air gun array. On the receiver side they will interfere with the upward traveling waves from the subsurface (UniGeo, 2012). Due to recent introduction of dual sensor technology, receiver-side ghosts can be efficiently removed by wave decomposition.

2.1.2 LINEAR COHERENT NOISE

Diffractions and refractions (far-field) are known as linear coherent noise. Diffractions may be caused by small scale inhomogeneties like pinch outs, faults and wedges as well as boulders on the sea floor (Olhovich, 1964). The case of a point scatter is shown in Fig. 2.2.

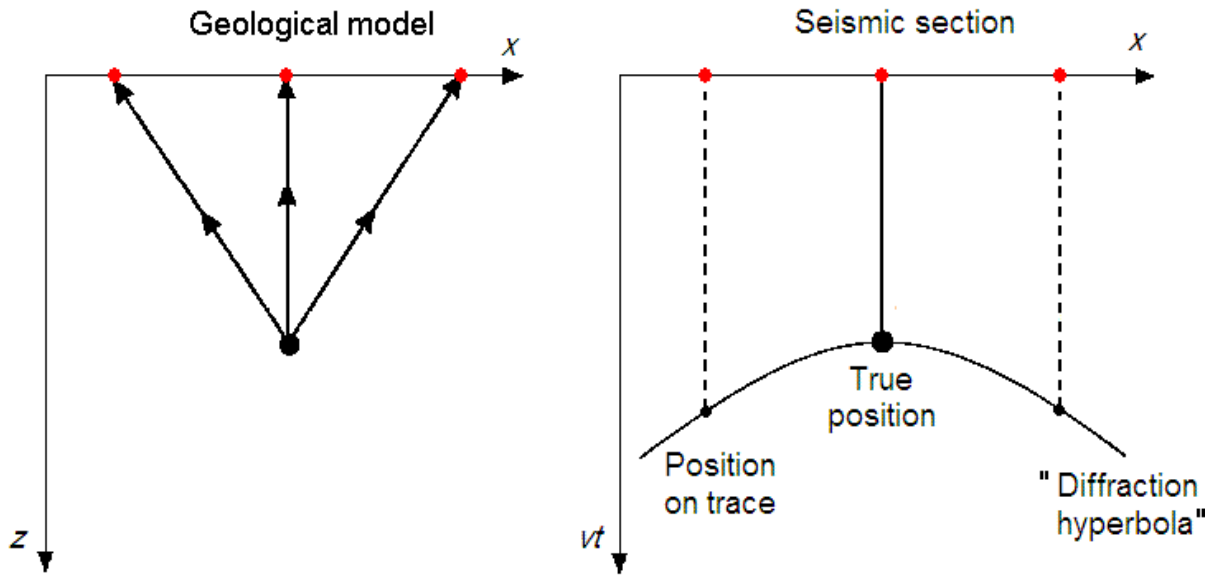

Figure 2.2: Schematic illustration of point diffractor (left) and zero-offset amplitude response given by the diffraction hyperbola (right). The flanks represent linear events (far-field) (modified from Stein and Wysession, 2003).

Diffractions can also form multiples if the energy is trapped in the water column. Diffractions usually follow a non-hyperbolic move-out, and are difficult to predict by multiple removal techniques and ray theory. An example of diffractions is shown in Fig. 2.3.

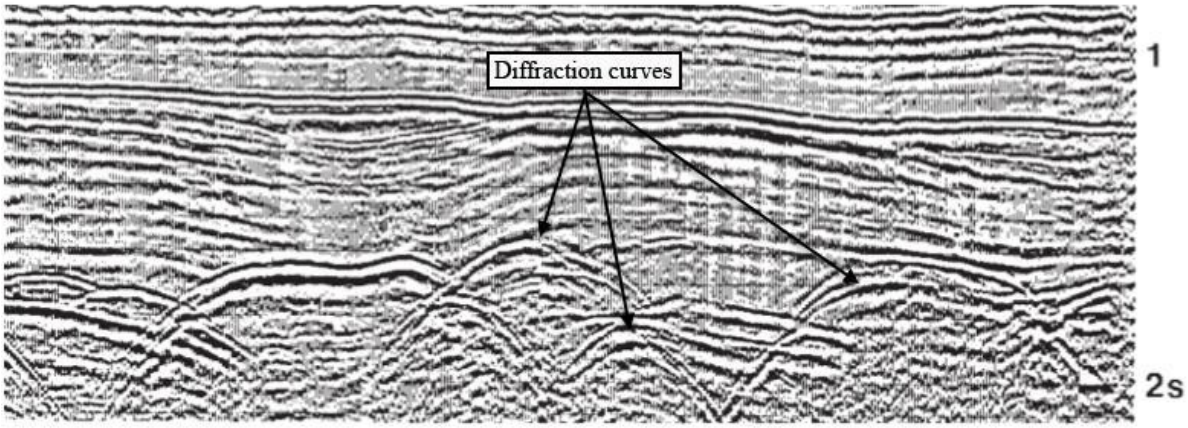

Figure 2.3: Example of diffraction hyperbolas in a seismic section (modified from Kearey, 2002).

Refractions may be found in the early parts of the records and occur when a layer acts as a good transmitter (Gelius and Johansen, 2010). The basic illustration of refraction is shown in Fig. 2.4.

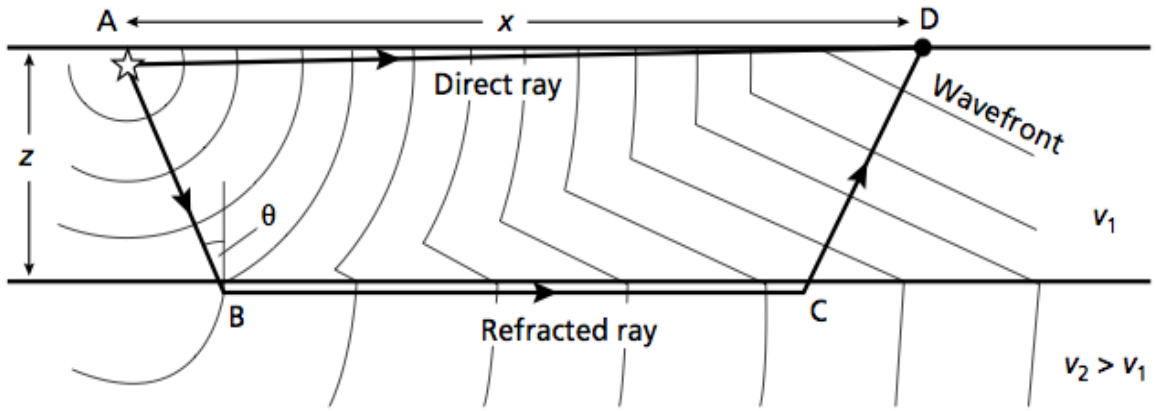

Figure 2.4: Schematic illustration of refraction in two layer earth model (Kearey, 2002).

Refractions occur when the angle of incidence is equal to the critical angle given by Snell's law. Such refractions are easy to remove in the early stage of processing. They give important information about shallow velocities on land data. On seismic section refractions will appear as straight lines crossing the reflected events.

2.1.3 AMBIENT NOISE

The unpredictable part of the data, characterized by a wide range of frequencies and a relatively flat amplitude spectrum, is known as ambient noise. After stacking, this type of noise is generally minimized (Elboth et al., 2010). Background noise like rain, vibration of machinery and tides are of high frequencies and can be removed by applying low band-pass and high band-pass filters (Gelius and Johansen, 2010; Yilmaz, 2001).

2.1.4 SWELL NOISE

It is difficult to put swell noise into any category but based on its amplitude spectra swell noise is a subtype of coherent noise. The main cause of swell noise is rough weather conditions during seismic acquisition. This noise is characterized by large amplitudes at low frequencies and is coherent to the number of hydrophones (cf. Fig. 2.5) (Elboth, 2010).

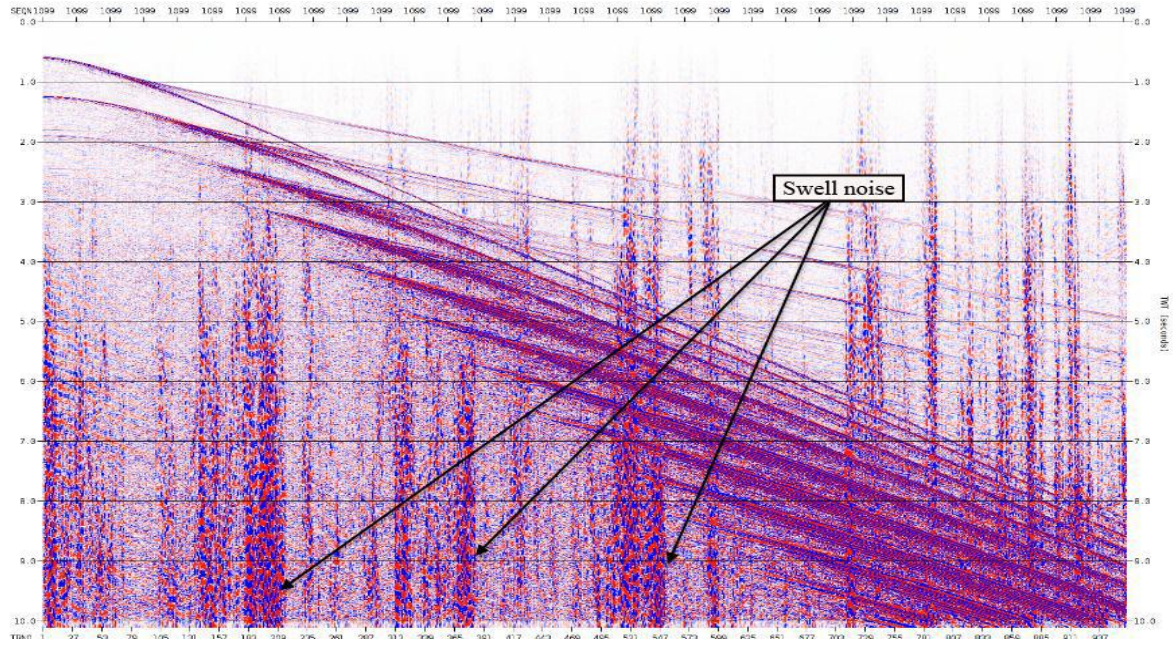

Figure 2.5: A shot gather with large amount of swell noise (Storbakk, 2012).

2.2 TYPE OF DIFFRACTIONS CONSIDERED IN THIS THESIS

In this thesis we will consider diffractions, and with special emphasize on water bottom multiples of diffractions. Such multiples can be strong and thus distort the reflection response of the subsurface. The question is then if possible techniques do exist to eliminate or minimize these multiples. In this work presented here, two different methods will be investigated: (i) Plane-wave destruction in the tau-p domain (Taner and Fomel, 2006) and (ii) Common reflection surface (CRS) technique (Jäger et al., 2001; Asgedom et al., 2011c).

In the following we give a brief discussion of typically cases where diffractions are generated.

2.2.1 DIFFRACTION CAUSED BY GLACIAL DEBRIS

Most of the marine seismic data acquired in Greenland consist of multiples of primary diffractions, generated by iceberg drift sourcing and glacial debris (Travis and Woodburn,

2010). These diffractions show high amplitudes compared to the underlying primary signals (cf. Fig. 2.6).

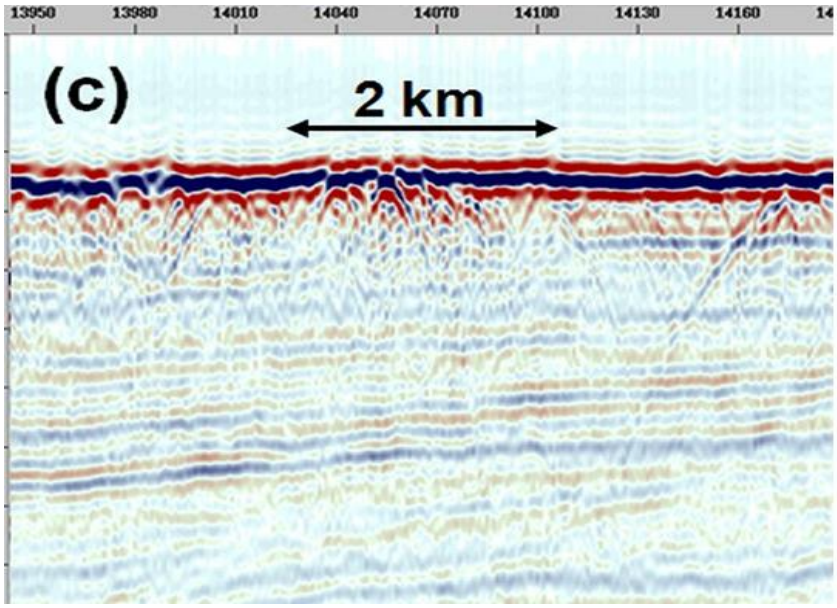

Figure 2.6: Diffraction caused by glacial debris, Greenland (Travis and Woodburn, 2010).

2.2.2 DIFFRACTION CAUSED BY ROUGH SEA-BED:

In the North Sea, most of the seismic data from the northern fields contain sea bed diffractions and associated multiples due to rough sea-bed topography. These diffractions and corresponding multiples are difficult to attenuate during seismic data processing. The sea-bed at the Norne field in the North Sea is dominated by glacial depositions which cause rough sea-bed topography (cf. Fig. 2.7).

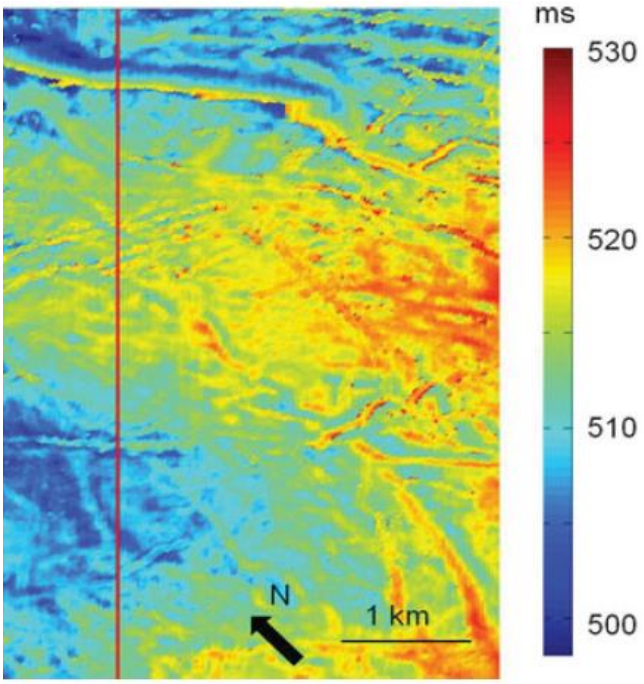

Figure 2.7: Sea-bed topography of the Norne field (Grude et al., 2013).

2.2.3 DIFFRACTION CAUSED BY SALT BODY

Diffractions are also caused by rough topography of salt bodies, diffractors in subsalt and complex fault structures. Figure 2.8 shows the complex synthetic dataset Sigsbee2A which consists of a salt body with rough top surface, reflectors and a complex fault system. Figure 2.9 shows the diffractions caused by the rough surface of salt body, diffractors in subsalt and complex fault system. The data represents a diffraction-enhanced stack based on the CRS technique, which is one of the two methods investigated in this thesis.

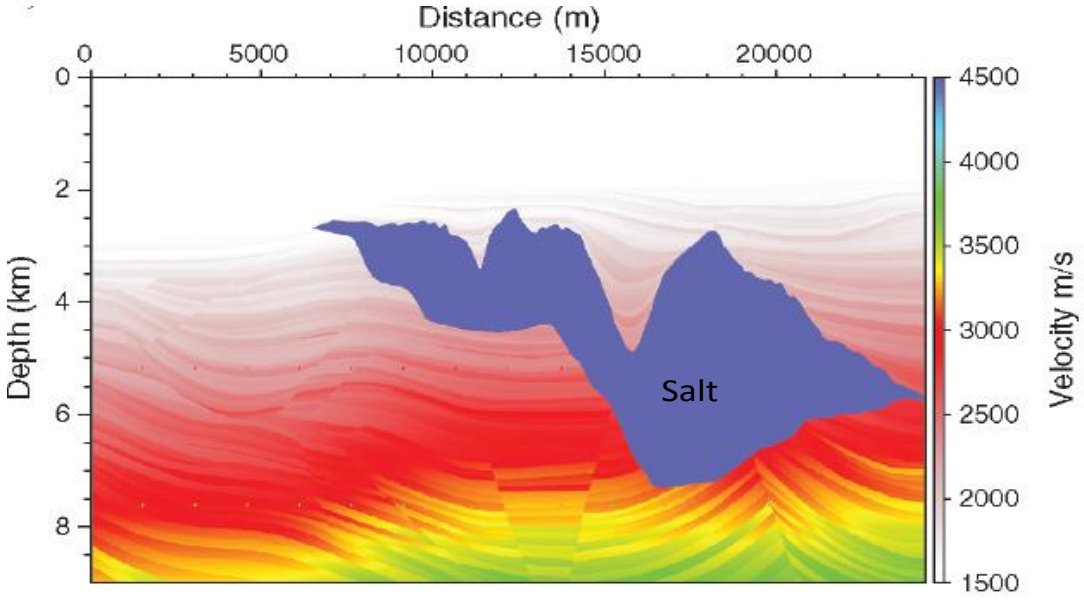

Figure 2.8: Synthetic dataset Sigsbee2A (Dell and Gajewski, 2011).

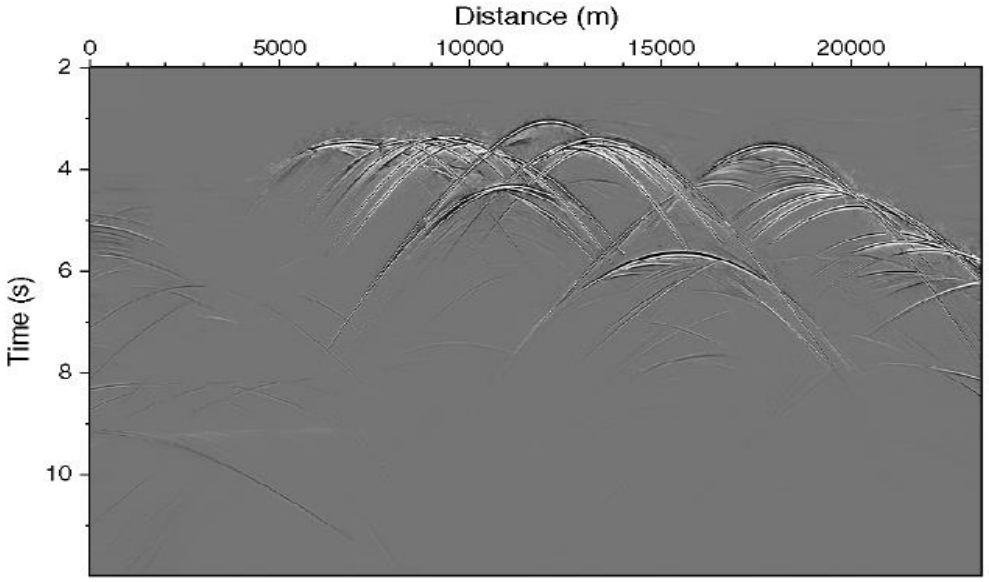

Figure 2.9: Stacked section after diffraction enhancement (CRS technique) showing diffractions caused by the rough salt surface and faults (Dell and Gajewski, 2011).

Chapter 3 GENERATION OF SYNTHETIC DATA

3.1 FINITE DIFFERENCE MODELING

Finite difference modeling is a precise and computes intensive method for forward modeling of the earth's response. In this work we used the finite-difference modelling (FDM) of PROMAX. A combined velocity and density model can be easily built by using the Interactive Velocity Editor. Since we consider 2D modelling, the subsurface will be represented by a two dimensional grid. Each rectangular grid cell is approximated by constant velocity and density.

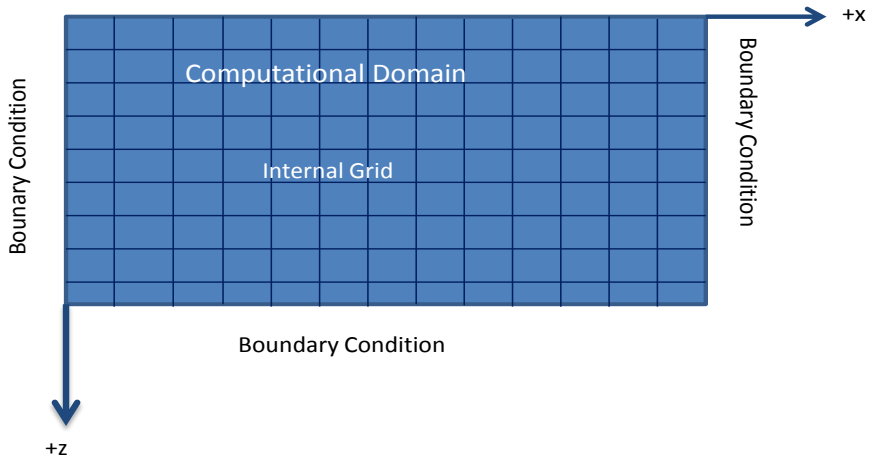

Figure 3.1: Two-dimensional grid of FDM simulating wave propagation.

Finite-difference modelling approximates numerically the equation of motion or the wave equation for a heterogeneous medium. FDM also needs numerical approximations along the boundaries called boundary conditions (cf. Fig. 3.1). These boundary conditions are typically as follows, absorbing boundaries along the vertical and lower boundaries and free boundary at the upper boundary.

The FDM program of PROMAX can be run in two different modes.

- Exploding Reflector: Post-stack zero-offset (ZO) modelling.
- Point Source: Pre-stack modelling of a source gathers.

The synthetic data employed here was generated using point-source mode. Two different models of varying complexity were considered. Model 1 is a two layer model (water layer and infinite half-space) with a scatterer placed on the seafloor. Model 2 is more complex involving a gently dipping seafloor, a two layered subsurface with a fault system and with the diffractor now buried in the overburden.

3.2 MODEL 1 (SIMPLE)

A survey containing a total of 750 shot points were generated using PROMAX, corresponding to the earth model described in Fig. 3.2. The acquisition and model parameters are listed in Table 3.1. A conventional 2D marine acquisition was simulated. Figure 3.2 shows a screen shot of interactive velocity editor of the FD program. During the modelling phase the water surface (upper surface of model) was assumed free, thus water bottom multiples were allowed to be calculated both for reflections and diffractions. Since a finite-difference code is employed, all relevant wave contributions are computed including the direct wave, peg-legs and refractions from sea floor. Since our model is two-dimensional (2D) there is an underlying assumption of a line source. Figure 3.3 shows an example of a typical shot record on source gather modelled by the program.

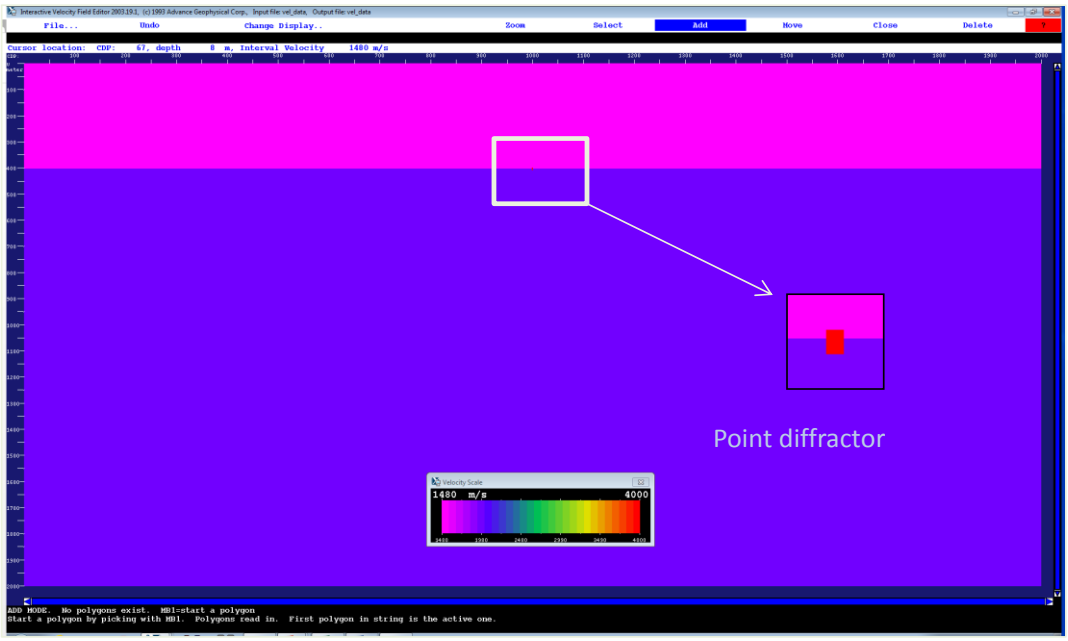

Figure 3.2: Interactive Velocity Editor (finite difference modelling) in case of Model 1.

Number of Shots	750
Number of receiver	900
Total number of CDP	2000
Source receiver minimum offset	250 m
Distance between two consecutive shots	25 m
Receiver interval	12.5 m
Velocity of point diffractor	4000 m/s
Depth of point diffractor	453 m
Velocity of first layer	1480 m/s
Velocity of second layer	2000 m/s

Table 3.1: seismic acquisition paramters.

3.2.1 SORTING IN SOURCE GATHERS

As already discussed, the output from FDM will be a series of shot records collected over the synthetic model (a total of 750 here). Figures 3.3 and 3.4 show examples of two such shot gathers.

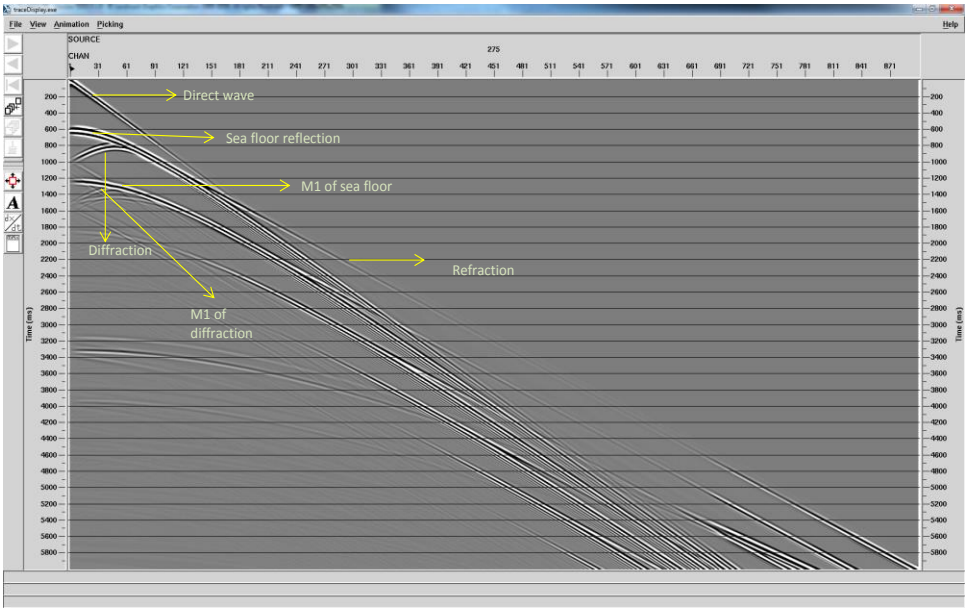

Figure 3.3: Modelled Shot gather # 275 with main events being labeled (M1 = first multiple).

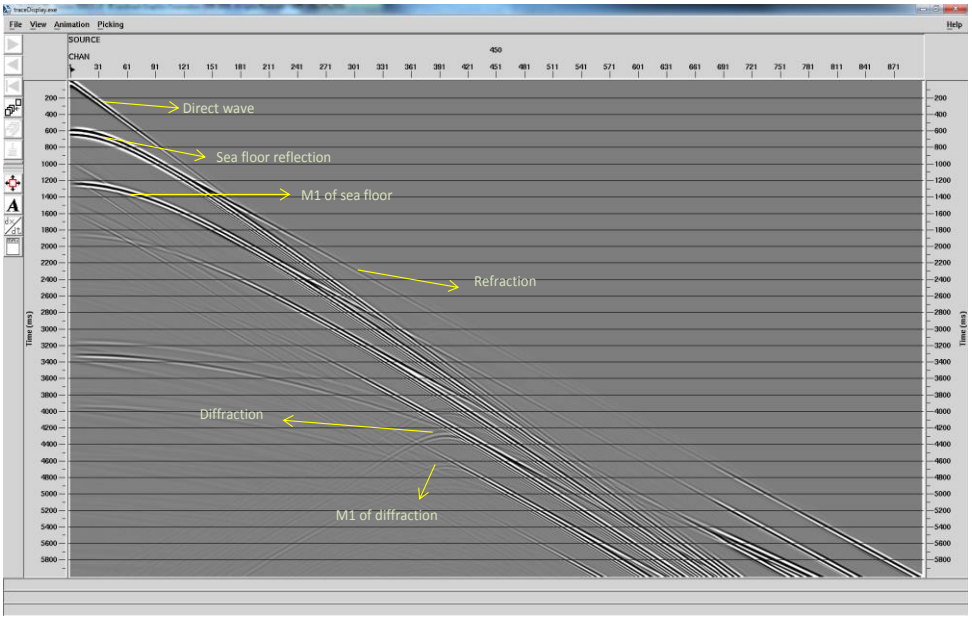

Figure 3.4: Modelled Shot gather # 450 with main events being labeled (M1 = first multiple).

In Fig. 3.3 the source is placed very nearby the scatterer, and the corresponding diffractions almost coincide with the primary reflection from the sea floor. Figure 3.4 represents a case where the source is far from the diffractor and the same two contributions are well separated.

3.2.2 SORTING TO CONSTANT OFFSET SECTION

Next, we sorted data to constant-offset (CO) sections.

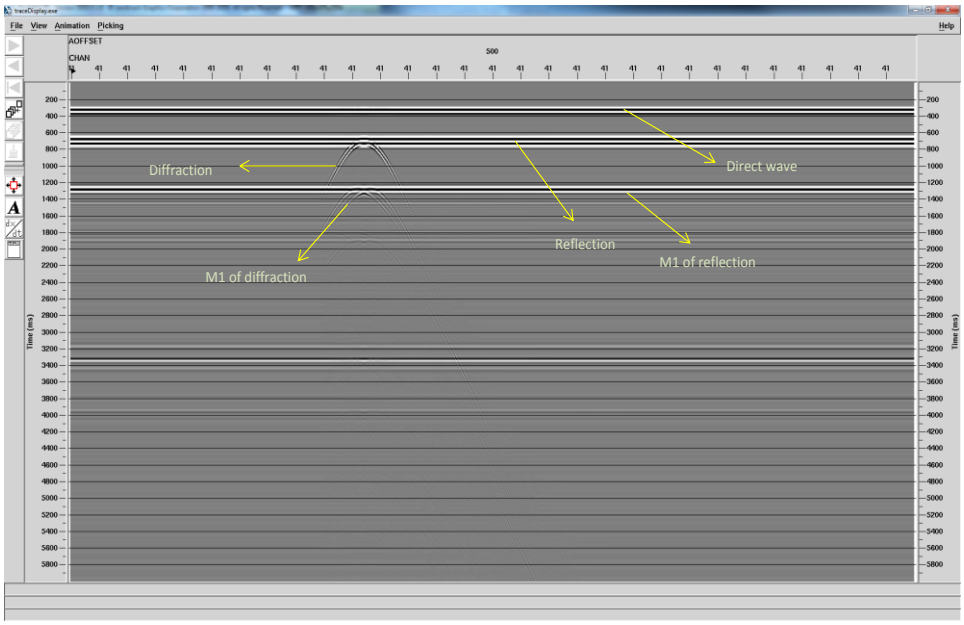

Figure 3.5: Constant offset section with reflection and diffraction responses (offset 500m).

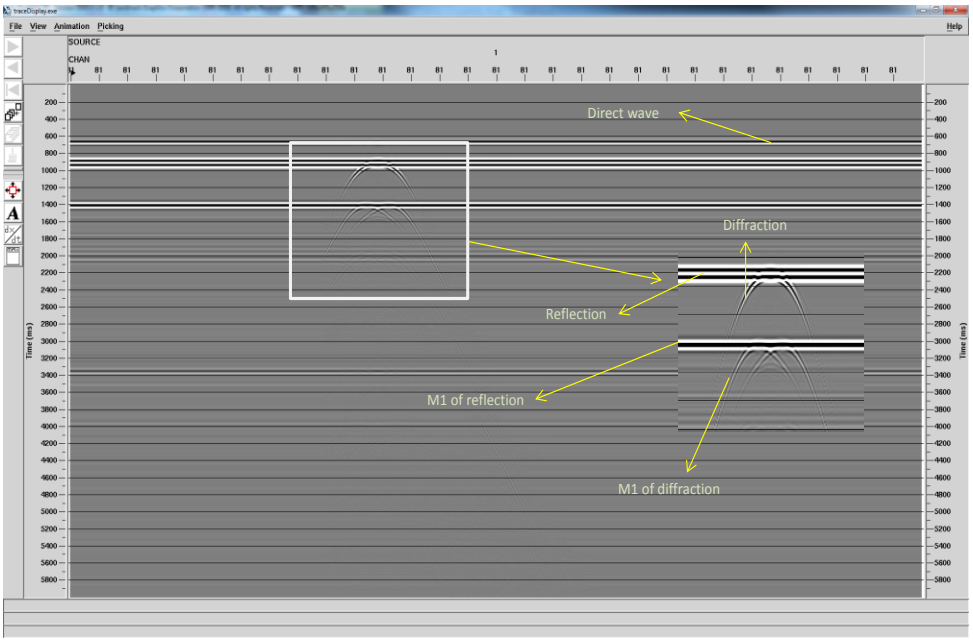

Figure 3.6: Constant offset section with reflection and diffraction responses (offset 1000m).

Figures 3.5 and 3.6 show the seismic responses for respectively an offset of 500 m and 1000 m. Due to the horizontal layer, reflections and associated multiples appear as flat events for both offsets. However, the diffractions still manifest as non-linear coherent events. Thus, unlike the shot domain, the two types of main events are now more separable. In Fig. 3.6, representing a larger offset, the two 'branches' of the multiples of diffraction can be easily seen.

3.2.3 SORTING TO COMMON MIDPOINT GATHER

We also checked how well the reflection and diffracted events separated in the CMP domain. Figure 3.7 shows the gather obtained for CMP 850. The separations between the two events indicate that the midpoint is further away from the diffractor. If the CMP is just above the diffractor, it will be difficult to distinguish between reflections and diffractions (cf. Fig. 3.8). Thus we make similar case of observations as in case of data in the shot domain. If the midpoint falls close to the location of the point scatter, the reflected and diffracted events do almost coincide (cf. Fig. 3.8). If the midpoint moves away, events separate well in time (cf. Fig. 3.7).

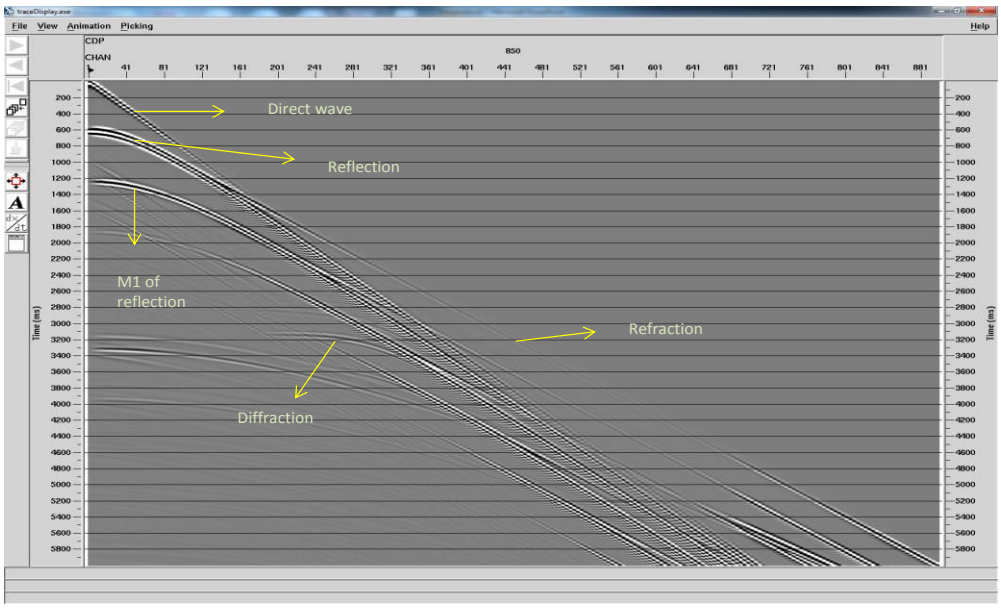

Figure 3.7: CMP gather with seismic events (CMP # 850).

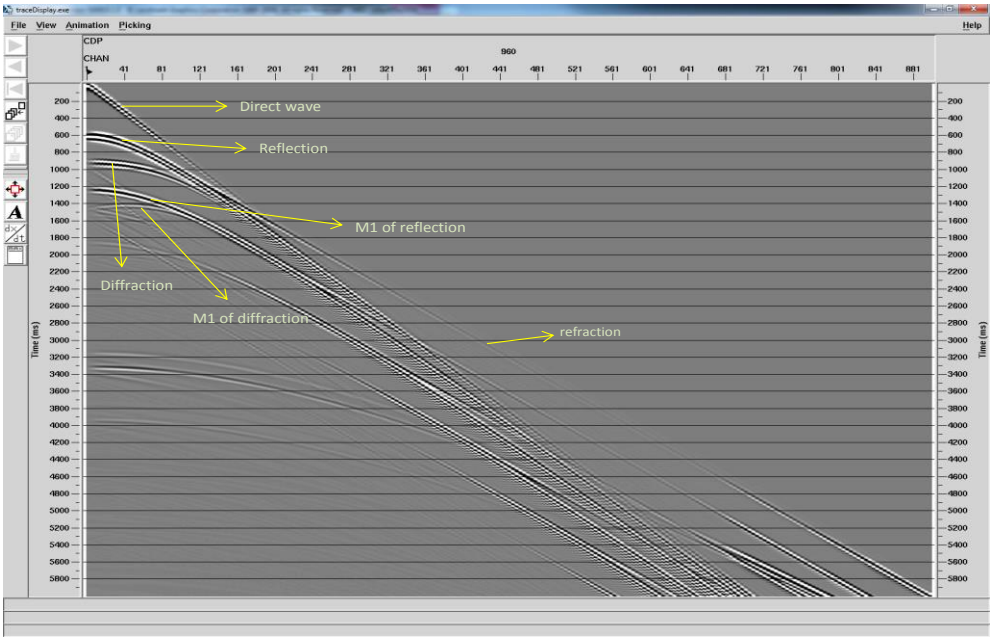

Figure 3.8: CMP gather with seismic events (CMP # 960).

3.3 **MODEL 2 (COMPLEX)：**

Figure 3.9 shows the corresponding velocity model generated by using the Interactive Velocity Editor of the Finite Difference Modelling (FDM) program in PROMAX. The acquisition parameters are listed in table 3.2. The model consists of a dipping layer; a faulted structure layer and a buried point diffractor (cf. Fig. 3.9).

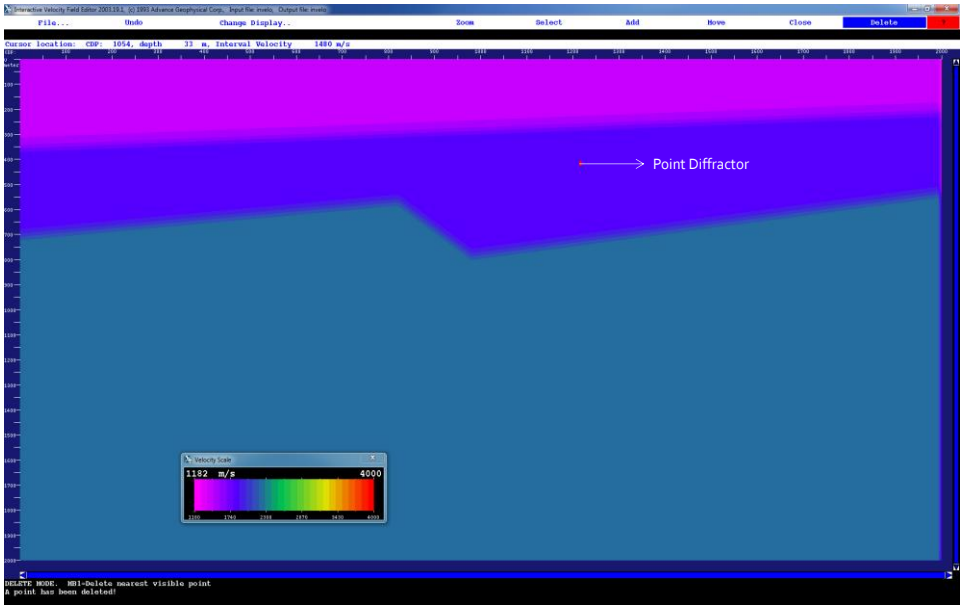

Figure 3.9: Velocity model in case of Model 2.

Number of Shots	750
Number of receivers	900
Source receiver minimum offset	250 m
Shot interval	25 m
Receiver interval	12.5 m
Velocity of first layer	1480 m/s
Velocity of second layer	1850 m/s
Velocity of third layer	2250 m/s
Depth of point diffractor	451 m
Velocity of point diffractor	4000 m
Total number of CDP	2000

Table 3.2: Seismic acquisition parameters (Model 2).

3.3.1 SORTING TO SOURCE GATHERS

Figures 3.10 and 3.11 are examples of two shot gathers modelled by using FDM in PROMAX.

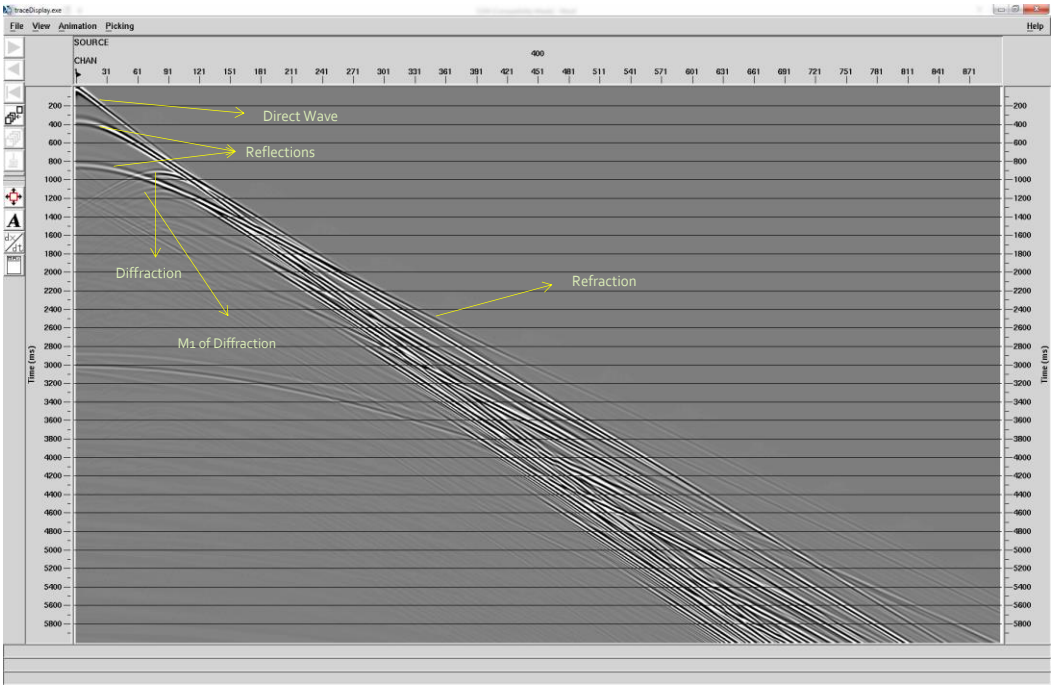

Figure 3.10: Modelled Shot gather # 400. Seismic events are being labelled (M1 = first multiples).

In Fig. 3.10 the source is placed near the diffractor and both reflections and diffractions are clustered in the same region with some overlap for smaller offsets. However, if the source is located further away from the diffractor, this will no longer be the case (cf. Fig. 3.11).

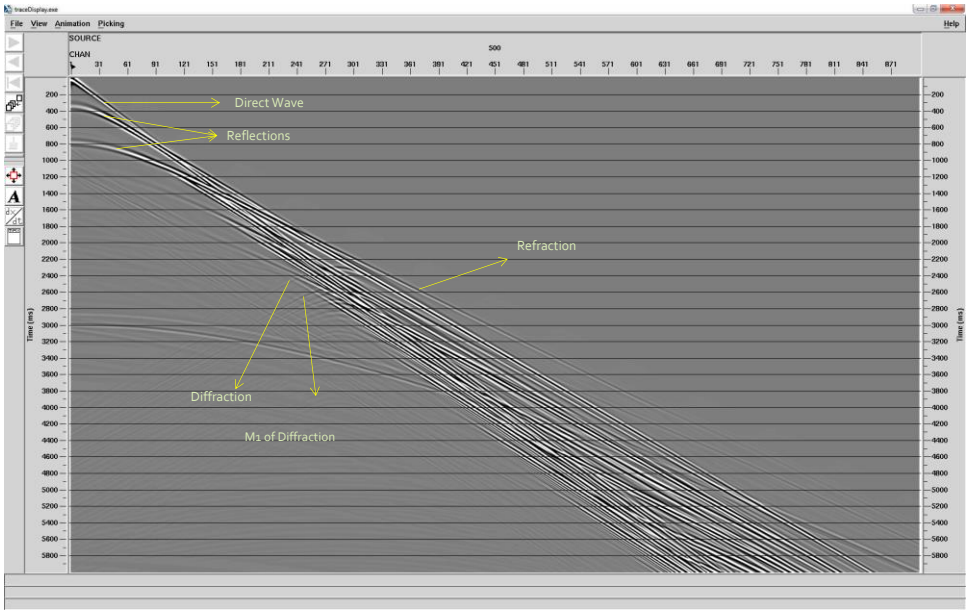

Figure 3.11: Seismic events modelled for shot # 500 (M1 = first multiple).

3.3.2 SORTING TO CONSTANT OFFSET SECTION

As in case of model 1, we also sorted data into constant-offset sections to check how the various events separate.

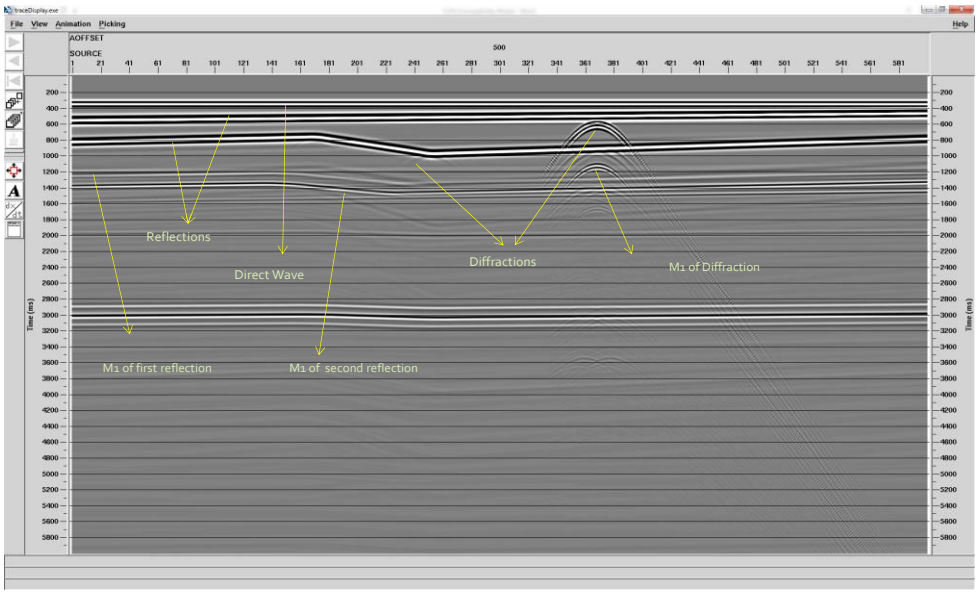

Figure 3.12: Constant offset section with reflections and diffractions (offset 500 m).

Figures 3.12 and 3.13 show constant offset sections at an offset of 500 m and 1000 m, respectively. Due to the complex model, reflections appear as non-flat events for both offsets whereas diffractions manifest themselves as non-linear coherent events. As offset increases it can be seen that the apex of diffractions becomes more flat and that the direct wave and primary reflection from the sea-floor are closer in time (cf. Fig. 3.13).

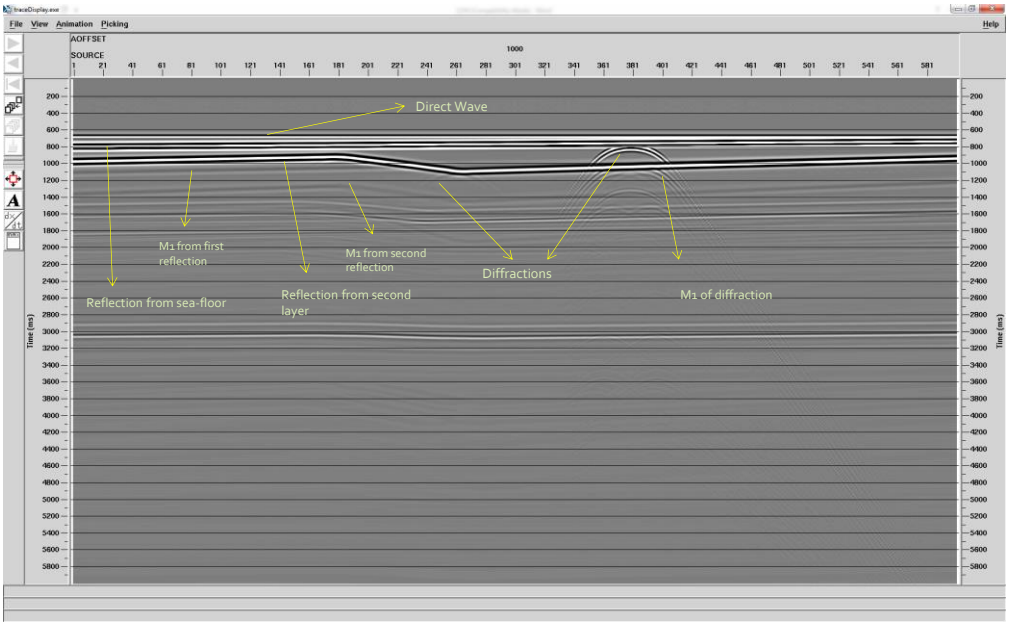

Figure 3.13: Constant offset section with reflections and diffractions (offset # 1000 m).

3.3.3 SORTING TO COMMON MIDPOINT GATHER:

Finally, we sorted the data into common mid-point gathers to see how well the primary events are being separated in the CMP domain. Figure 3.14 shows CMP gather 1100. Primary events of reflections and diffractions can be easily separated if the midpoint falls further away from the diffractor (cf. Fig. 3.14). If the CDP is just above the point diffractor, it will be difficult to distinguish between reflections and diffractions (cf. Fig. 3.15). Similar observations have been obtained in the shot domain (cf. Fig. 3.10 and 3.11).

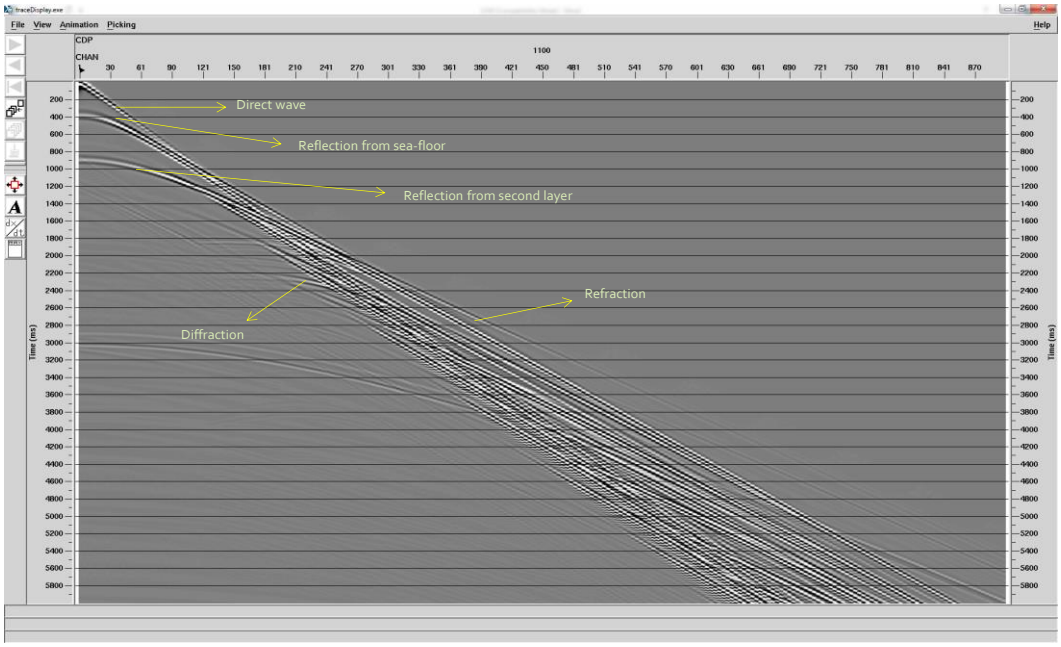

Figure 3.14: CMP gather with seismic events (CMP #1100).

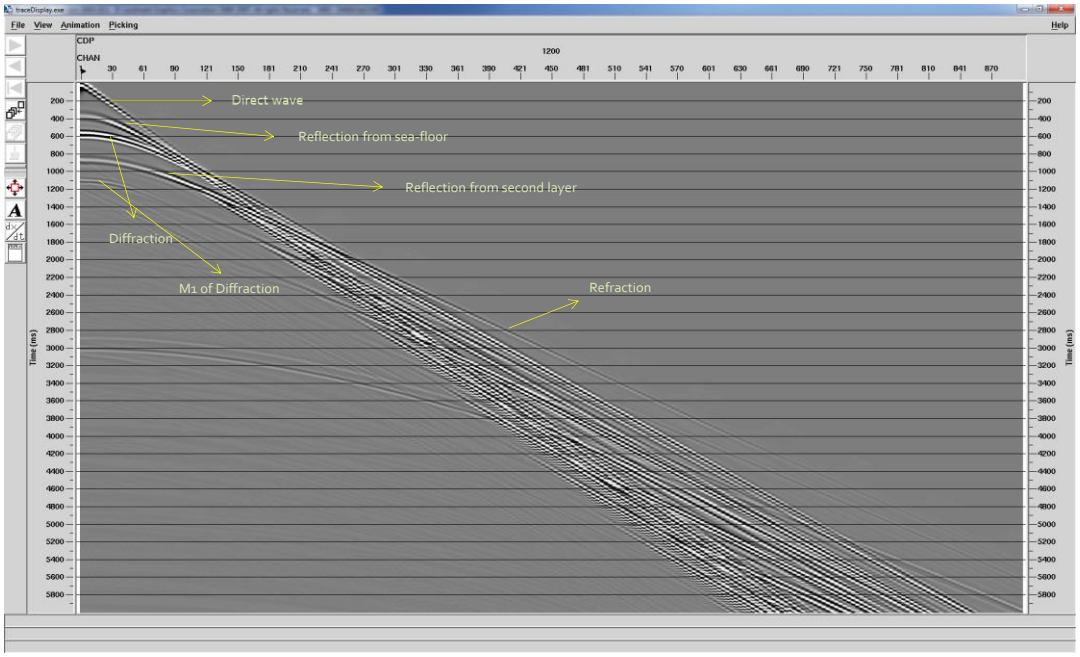

Figure 3.15: CMP gather with seismic events (CMP # 1200).

Chapter 4 PROCESSING METHODS

In this chapter we will discuss the basics of the two methods investigated in this thesis: i) Plane-wave destruction in the tau-p domain and ii) modified CRS technique.

4.1 PLANE-WAVE DESTRUCTION IN THE (TAU-P) DOMAIN

The basic of this technique is built on i) tau-p transformation and ii) plane wave destruction filtering. We will therefore start by discussing these two concepts.

4.1.1 TAU-P TRANSFORMATION

The tau-p transform or slant stack, transforms the data from space - time (x - t) domain into a constant dip *p* and zero offset intercept time τ (Durrani and Bisset, 1984). In the τ-*p* domain all events along a constant p trace have the same ray parameter p. This parameter represents the apparent horizontal slowness dt/dx or slope of a plane-wave in the space-time domain. The events can therefore be separated according to angle of incidence since each transformed trace represents a fixed angle of incidence at the surface. In case of a flat seafloor, the periodicity of water bottom multiples is preserved in the τ-*p* domain (Tatham et al., 1983).

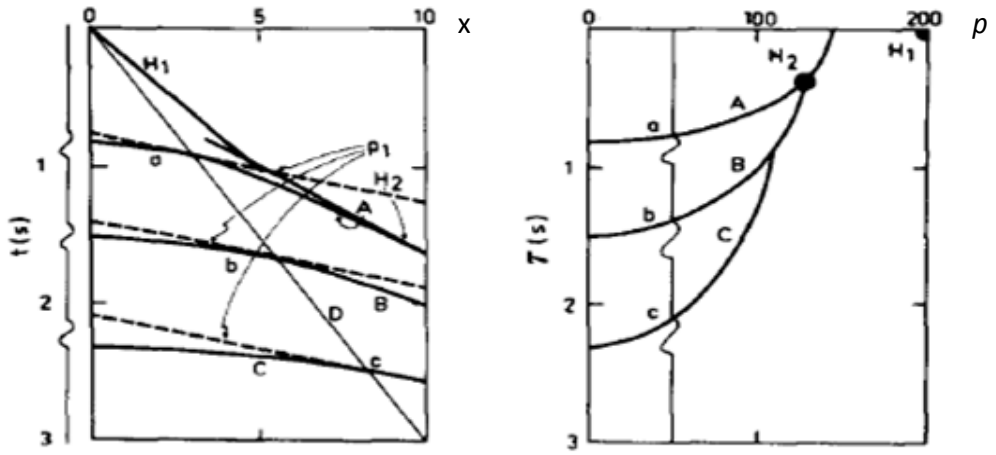

Figure 4.1: Construction of the tau-p (slant stack) transform (Tatham et al, 1982).

Figure 4.1 shows how seismic events are mapped from the space-time domain to the tau-p domain. The three events A, B and C represent reflections. Each point on a reflection hyperbola can be approximated by a local plane-wave like H_2 in case of reflection A. Such a plane wave will map to a point in the tau-p domain. By considering all local plane-waves defining a reflection it can be shown that they fall along an elliptical curve in the transformed domain. In Fig. 4.1 H_1 represents the direct wave which is linear in space-time thus representing a plane-wave. Every linear event will be mapped to a point in the tau-p domain. Thus the τ-p transformation can be regarded as plane-wave decomposition. An example of τ-p transformation of a CMP gather is shown in Fig. 4.2.

A plane-wave in the space-time domain can be expressed by the linear moveout

$$\tau = t - px \tag{4.1}$$

where x is offset, t is time, p is ray parameter and τ intercept time.

The τ-p transformation can now be expressed mathematically by

$$s(p, \tau) = \Sigma_x \, p(x, \tau + px) \tag{4.2}$$

Where $p(x, t)$ represents input data and the summation is carried out along the spatial axis x.

The output $s(p, \tau)$ represents now a plane-wave in space-time with slope p and intercept time τ (corresponding to x=0).

Like in the case of a Fourier Transform, an inverse tau-p transform can be constructed. It takes the form

$$p\ (x,t) = \Sigma_p\, s(p, \tau - px) \tag{4.3}$$

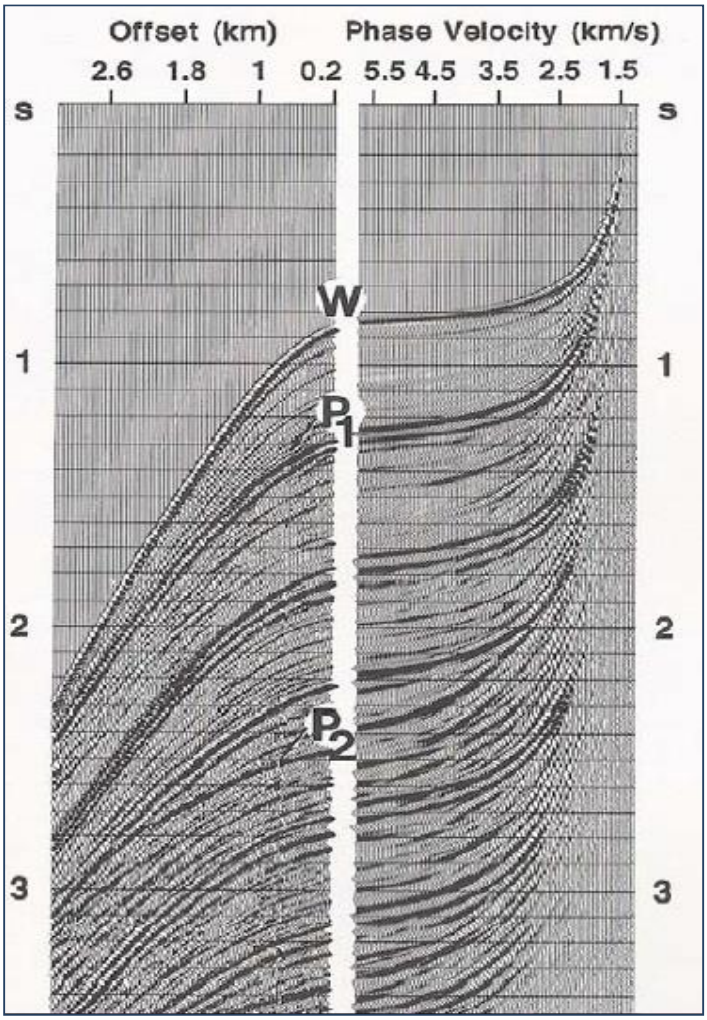

Figure 4.2: CMP gather left with water bottom reflection (W) and two other primary events (p_1 and p_2) and associated multiples. The corresponding τ-p gather is shown to the right (Yilmaz, 2001).

In case of 2D data and line sources the inverse τ-p transformations as stated in Eq. (4.3) lacks amplitude correction factors. Thus by taking τ-p transformation of one of the modelled shot records followed by an inverse τ-p transformation and finally subtracting the output from the original source gather will give a residual gather (cf. flow diagram in Fig. 4.3).

Figures 4.4, 4.5 and 4.6 represent respectively input shot record, the τ-p transformed gather and the output after inverse τ-p. Finally by subtracting the result of Fig. 4.6 from that of Fig. 4.4 the residual gather as shown in Fig. 4.7 is obtained. Ideally this latter gather should be zero, but due to imperfections in the inverse τ-p transform, various minor artifacts are created.

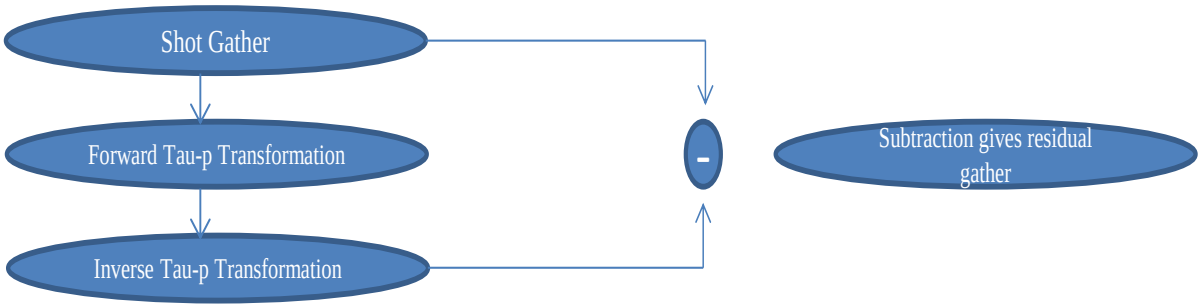

Figure 4.3: Flow diagram for testing of forward and inverse tau-p transformation.

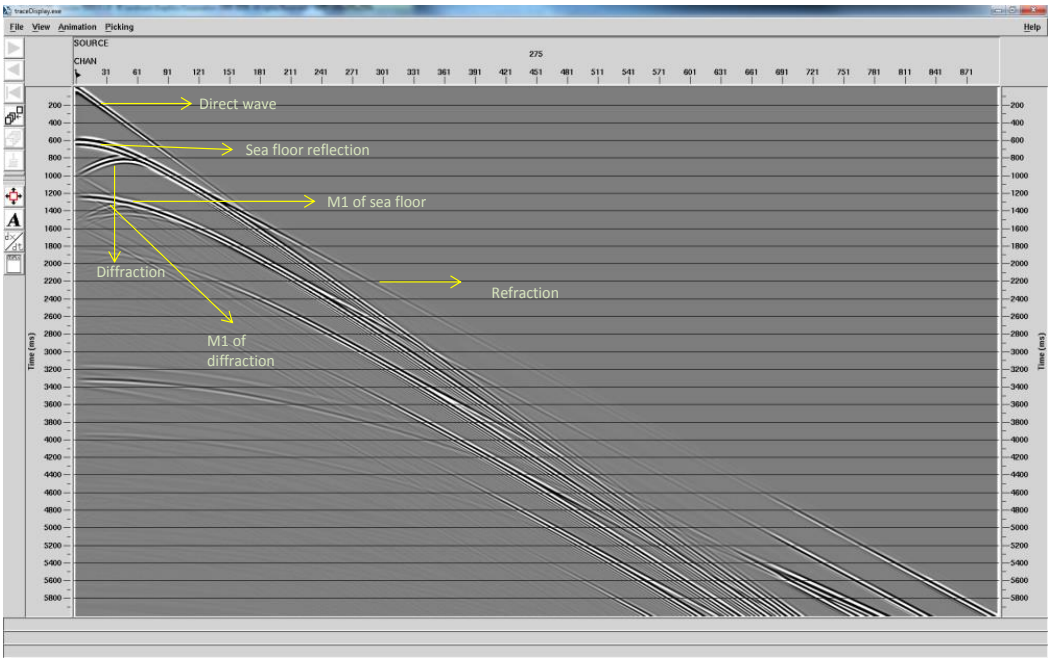

Figure 4.4: Shot gather used as input (shot # 275).

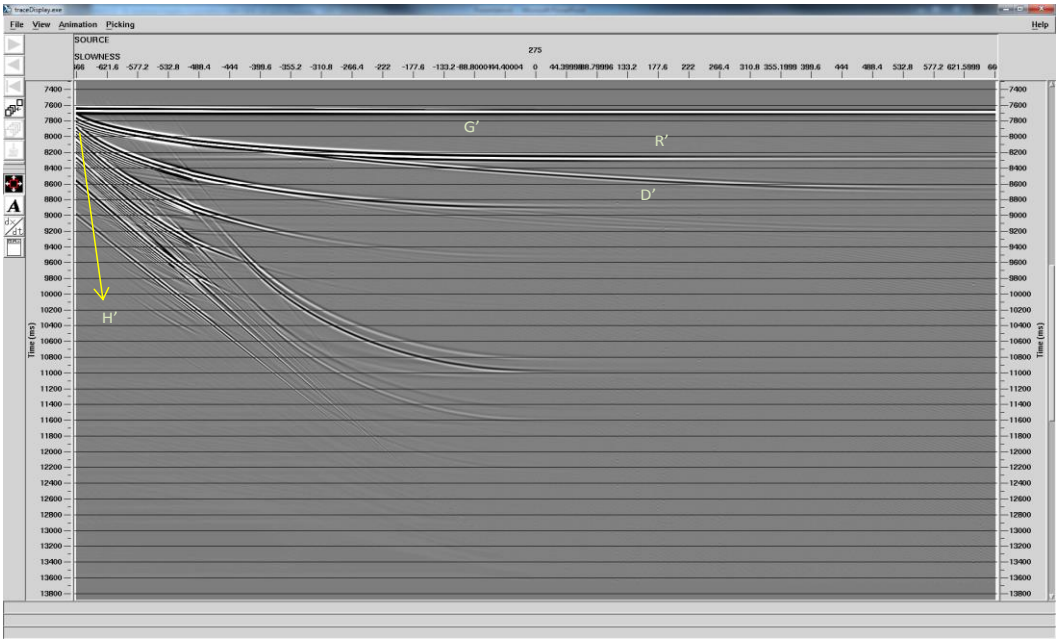

Figure 4.5: Tau-p transformation of shot gather in Fig. 4.4.

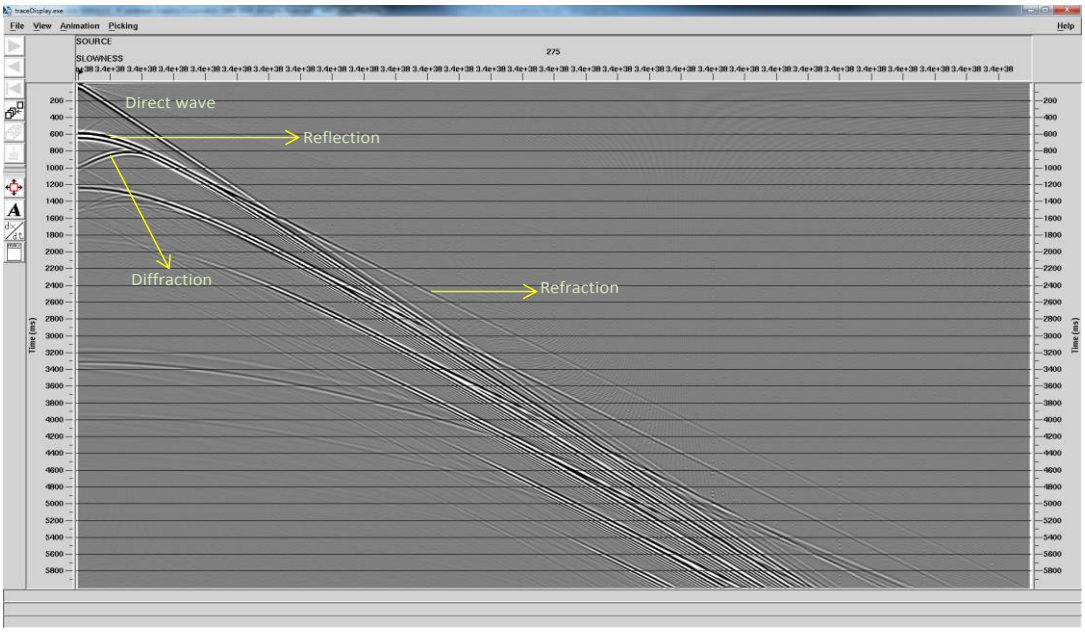

Figure 4.6: Result after inverse tau-p of gather in Fig. 4.5.

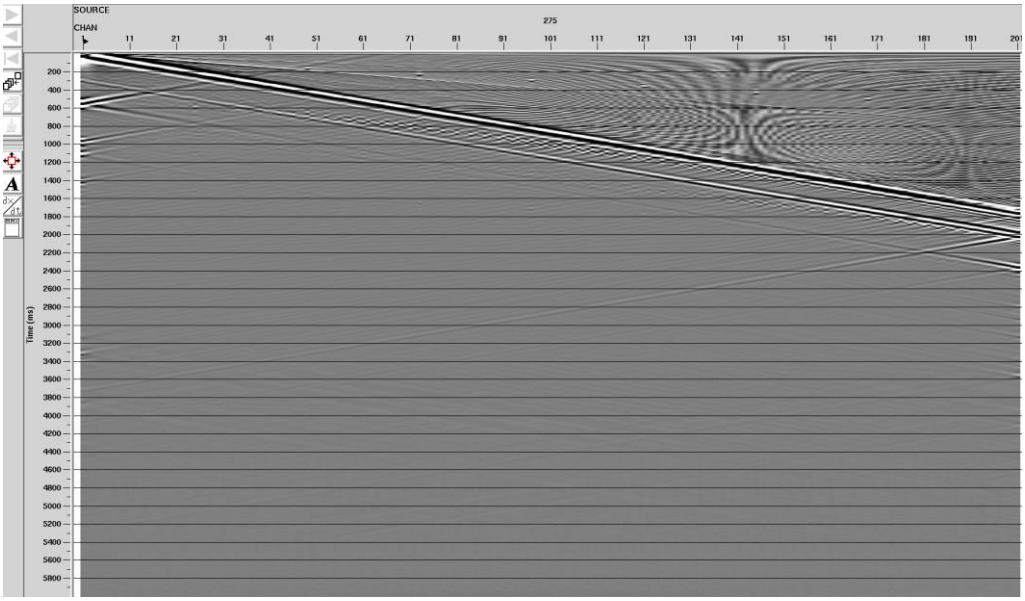

Figure 4.7: Residual gather.

4.1.2 PLANE WAVE DECOMPOSITION

In Case of Plane-wave illumination a stack of layers will generate a family of reflected plane-waves, whereas scatterers still will generate the well-known diffraction responses. Sorting data into CO sections is a simple way to generate a quasi plane-wave illumination. We have also seen from earlier discussions, that diffractions and reflections separate better after such sorting. A more rigorous approach to synthesize plane-wave illumination is to go via the tau-p transformation. By transforming a set of source records, a plane-wave section can be constructed from selecting only traces with the same *p* value (i.e. common-*p* section). Thus a whole family of common-*p* sections can be constructed, each of them is repeating plane-wave illumination at different angles of incidence.

Two basic principal are used to generate such plane-wave sections, law of superposition and law of reciprocity. Law of reciprocity predicts that source and receiver locations can be interchanged while law of superposition combines different seismic records to give us plane wave records.

A summary of the procedure is as follows:

- Generate common source records by using law of reciprocity.
- Tau-p of each common source record.
- Sort into common *p* sections.
- Apply plane wave destruction filter on each constant *p* section.

A plane-wave destruction filter is designed to remove linear events from a seismic section. Thus after filtering, each constant-*p* section will appear with diffractions only (at least ideally). By subtracting these contributions from the original data in the transformed domain, followed by an inverse tau-p transform, reflection only data can be obtained.

A discussion of the design and details of the plane-wave destruction filter is outside the scope of this thesis work. For additional information, the reader is referred to Fomel (2002).

4.1.3 SCHEMATIC OF COMPLETE METHOD

After having described the basics of respectively the tau-p transformation and the plane-wave destruction filtering, we are now in the position to describe the complete method. The overall computational flow is given in Fig. 4.8.

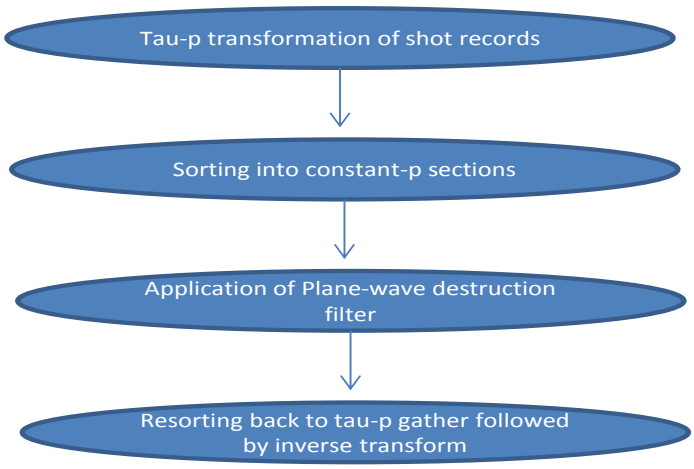

Figure 4.8: Computational flow.

In order to extend the range of shot records to comply with a split-spread geometry the reciprocity principal is applied. A typical constant-*p* section is shown in Fig. 4.9a. In case of a 1D earth model the corresponding reflections will transform to horizontal events in each such constant-*p* section. However diffractions will transform to events smeared out in the same sections. After applications of plane-wave destruction filter, the horizontal events can be removed. Figure 4.9b shows an example of diffractions only surviving in the tau-p domain after this filtering. Two different types of output can now be obtained. By sorting this diffracted energy back into p-τ gathers followed by inverse transformation gives diffraction enhanced data. Alternatively, by subtracting this kind of data from the original data, the contribution from the diffractions (and associated multiples) can be removed.

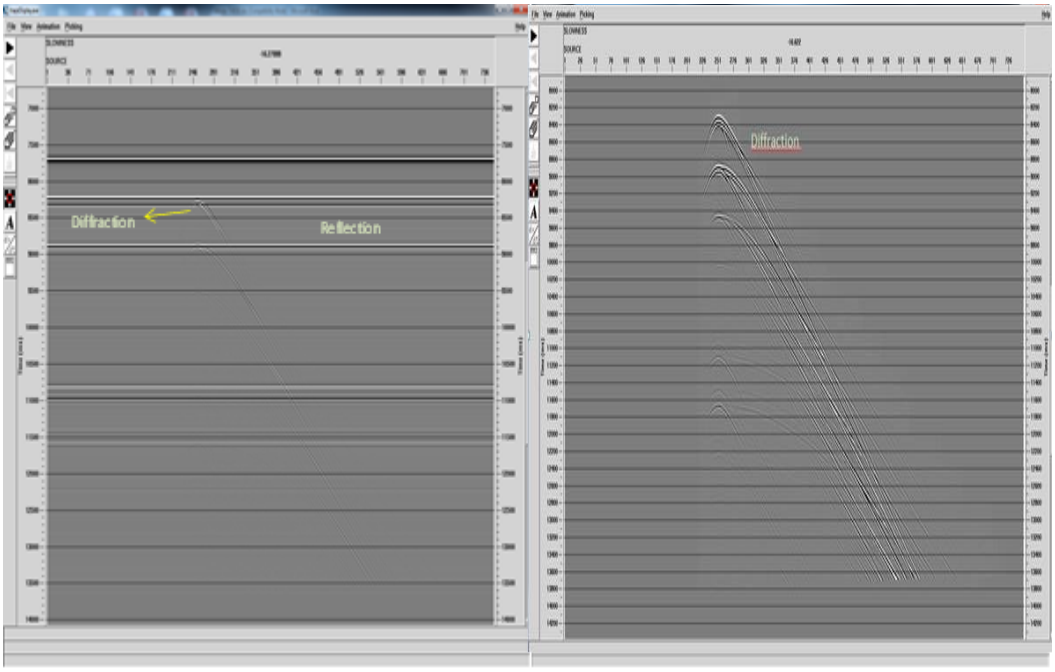

a): p = -16.28

b): Diffractions only preserved after plane-wave destruction filtering of (a)

Figure 4.9: Common-p section (a) before and (b) after plane-wave destruction filtering.

4.2 THE COMMON REFLECTION SURFACE (CRS) TECHNIQUE

4.2.1 INTRODUCTION

The Common Reflection Surface (CRS) technique (Jäger et al., 2001) is an alternative approach to the common mid-point (CMP) method to further enhancement of the signal to noise ratio. CRS also gives additional kinematic parameters which are useful for imaging purposes. In CRS, reflections are enhanced by stacking along the CRS move-out. A similar procedure is carried out for enhancement of diffractions (Faccipieri et al., 2013).

In conventional seismic processing we enhance reflected events but these events do not carry information about the small geological features such as pinchouts, faults and fractures. For such type of events, seismic diffractions are needed. Since diffractions are weaker than reflections it is necessary to enhance such events if to be used. One such enhancement method can be constructed from a modified version of the CRS technique (Faccipieri et al., 2013).

4.2.2 CMP AND CRS COMPARISON

The common mid-point analysis is a conventional way to generate a stack of the seismic data. The travel time equation used for reflection in a CMP is given on the form

$$t = (t_0^2 + \frac{2h^2}{V_{NMO}^2})^{1/2} \qquad (4.4)$$

Where t_0 is the ZO traveltime, h is the half-offset and V_{NMO} represents the NMO-velocity.

Consider now the case of an arbitrary reflector (Figure. 4.10). We introduce the concept of a ZO central ray and use a paraxial approximation to obtain the travel time expression for a nearest ray within a given offset. The new travel time equation (4.5) is the generalization of equation (4.4) where the midpoint coordinate m can be varied. To properly take into account the shape of the reflector, new parameters have to be introduced like the local slope of the

traveltime curve *p* and its curvature. The curvature move-out velocity V_{CMO} in equation (4.5) depends upon the curvature unlike the NMO velocity (Mann et al., 2007).

$$t^2(m,h) = t_0^2 + \frac{h^2}{v^2_{NMO}} + \frac{(m-m_0)^2}{v^2_{CMO}} + 4t_0p(m-m_0) + 4p^2(m-m_0)^2 \qquad (4.5)$$

In Eq. (4.5) m represents the mid-point coordinate of the paraxial ray and m_0 that of the ZO reference ray (cf. Fig. 4.10).

Morover, *p* represents the slope.

4.2.3 CRS METHOD FOR REFLECTION

The CRS method can provide a generalized zero offset section with high signal to noise ratio and also give additional information about attributes of geological structures. This is because the CRS method interpolates the subsurface reflectors as a group of reflecting elements defined not only by points but also by curvature and dip. The CRS stacking operator uses information about source receiver pairs in the vicinity of the central CMP position where the final ZO trace will be constructed. An alternatively way of representing the CRS-equation in Eq. (4.5) is as follows (Jäger et al., 2001).

$$t^2(m,h) = [t_\circ + A(m-m_\circ)^2] + B(m-m_\circ)^2 + Ch^2 \qquad (4.6)$$

Where again $t_\circ$ is the traveltime of the ZO reference ray and h is the half offset of an arbitrary source-receiver pair with midpoint m (cf. Fig. 4.10).

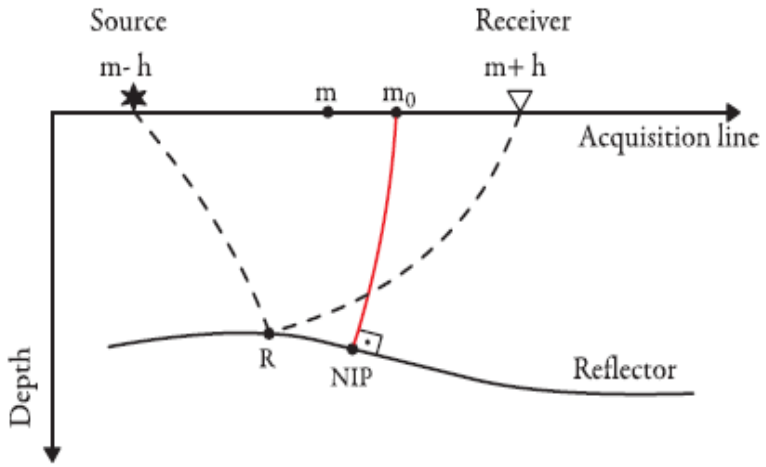

Figure 4.10: CRS geometry with paraxial source receiver pair surrounding the central ray at m_0 (Faccipieri et al., 2013.)

The coefficients A, B and C in Eq. (4.6) are defined as follows

$$A = 2\sin\beta/v_0\ , \quad B = 2t_0\cos^2\beta K_N/v_0, \quad C = 2t_0\cos^2\beta K_{NIP}/v_0 \tag{4.7}$$

where v_0 is the near surface velocity and β is the emergance angle of the ZO reference ray at m_0. Moreover, K_{NIP} represents the curvature of a hypothetical wavefront called NIP-Wave related with a point source located at the point where the normal ray is incident, and measured at m_0 (cf. Fig. 4.11). Finally K_N represents the curvature of a hypothetical wavefront called N-Wave which originates from a region in the area of the same normal incident point as an exploding reflector event (cf. Fig. 4.12) (Asgedom et al., 2011b).

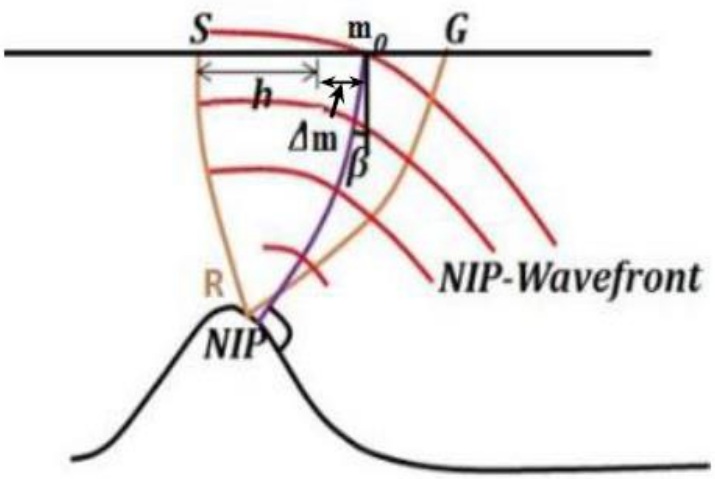

Figure 4.11: Definition of NIP (normal incident point) wavefront (modified from Asgedom et al, (2011c)).

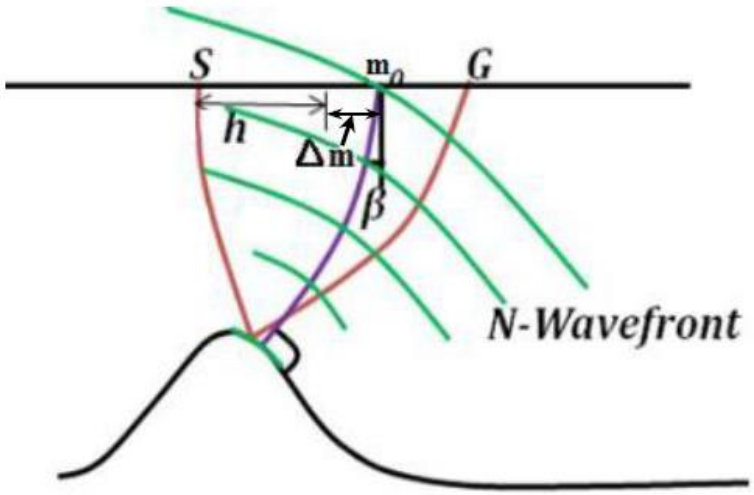

Figure 4.12: Definition of N (normal) wavefront (modified from Asgedom et al, (2011c))

In order to estimate the CRS parameters A, B and C, a two-step procedure is being employed as described below. This includes the combined use of the CMP and ZO domains (cf. Fig. 4.13).

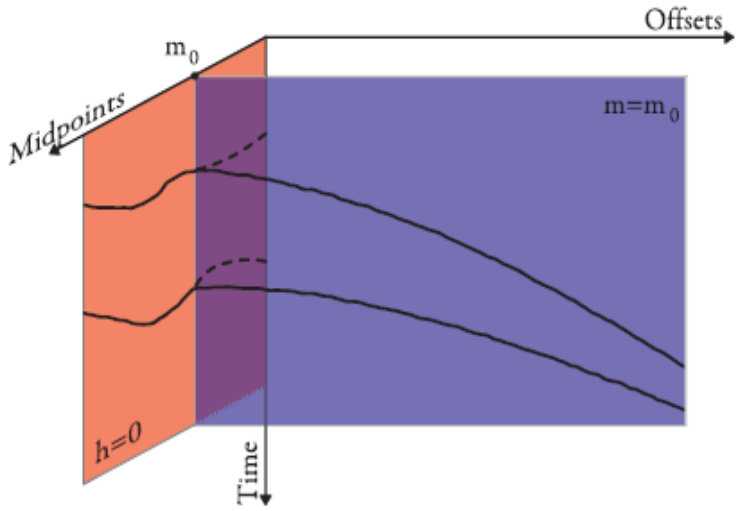

Figure 4.13: CMP ($m=m_0$) and ZO ($h=0$) slices through prestack data (Faccipieri et al., 2013.)

First we consider data sorted in the CMP domain ($m = m_0$) which gives the following simplified form of equation (4.6)

$$t^2(m_0, h) = t_0^2 + Ch^2 \qquad (4.8)$$

In this case the travel time equation depends only on parameter C which is estimated using semblance. This equation is similar to conventional velocity analysis where C is replaced by $4h^2/V^2_{NMO}$ in the CMP method. This shows that parameter C also carries information about the velocity model. Secondly, we consider data after stacking using $v_{NMO} = 2/(C)^{1/2}$ (i.e. ZO domain) obtained by setting h = 0 in Eq. (4.6).

$$t^2\,(m, 0) = [t_0 + A\,(m\text{-}m_0)^2] + B\,(m\text{-}m_0)^2 \qquad (4.9)$$

where the travel time equation now depends upon the two parameters A and B. A can be estimated by assuming B=0 for a small aperture and parameter B can be estimated by using a

larger aperture, employing the already known value of parameter A. In both cases, the parameters are estimated by semblance.

4.2.4 CRS METHOD FOR DIFFRACTIONS

The main purpose of CRS is to enhance reflected events, but this technique can also be modified to enhance diffractions. This can be done by considering a point diffractor as a limiting case where a reflector shrinks to a point. This case corresponds to coinciding NIP and N-waves, thus we set $K_N = K_{NIP}$. Introducing this condition, the diffraction counter part of Eq. (4.6) reads

$$t^2(m,h) = [\, t_0 + A(m-m_0)\,]^2 + C[\,(m-m_0)^2 + h^2] \qquad (4.10)$$

Thus in case of diffractions, only two parameters A and C are considered. Parameter C is calculated from Eq. (4.8) in the same way as in case of reflections. The parameter A can be estimated from the ZO diffraction stack by setting h=0 in Eq. (4.10).

$$t^2(m,0) = [t_0 + A\,(m-m_0)]^2 + C(m-m_0)^2 \qquad (4.11)$$

By using a coherency measure like semblance and stacking the already stacked data along the traveltime curve in Eq. (4.11), optimal values of A can be obtained *(Faccipieri et al., 2013).*

Chapter 5 DATA PROCESSING RESULTS

5.1 PLANE-WAVE DESTRUCTION IN THE TAU-P DOMAIN (SIMPLE MODEL)

The main steps of this technique are summarized in Fig. 5.1. The corresponding parameters used for the actual tau-p transformation are given in Table 5.1. As can be seen from Fig. 5.1 (and also discussed in previous sections) two alternatively processing branches exist: i) diffraction enhancement or ii) diffraction removal/attenuation. We will give examples of both types of output.

In the following we will illustrate the performance of the technique by considering the source gather corresponding to shot # 275 (cf. Fig. 5.2). In Fig. 5.2 we have labelled the following main events: direct wave (G), refraction from sea-floor (H), primary reflection from sea-floor (R) and primary diffraction (D).

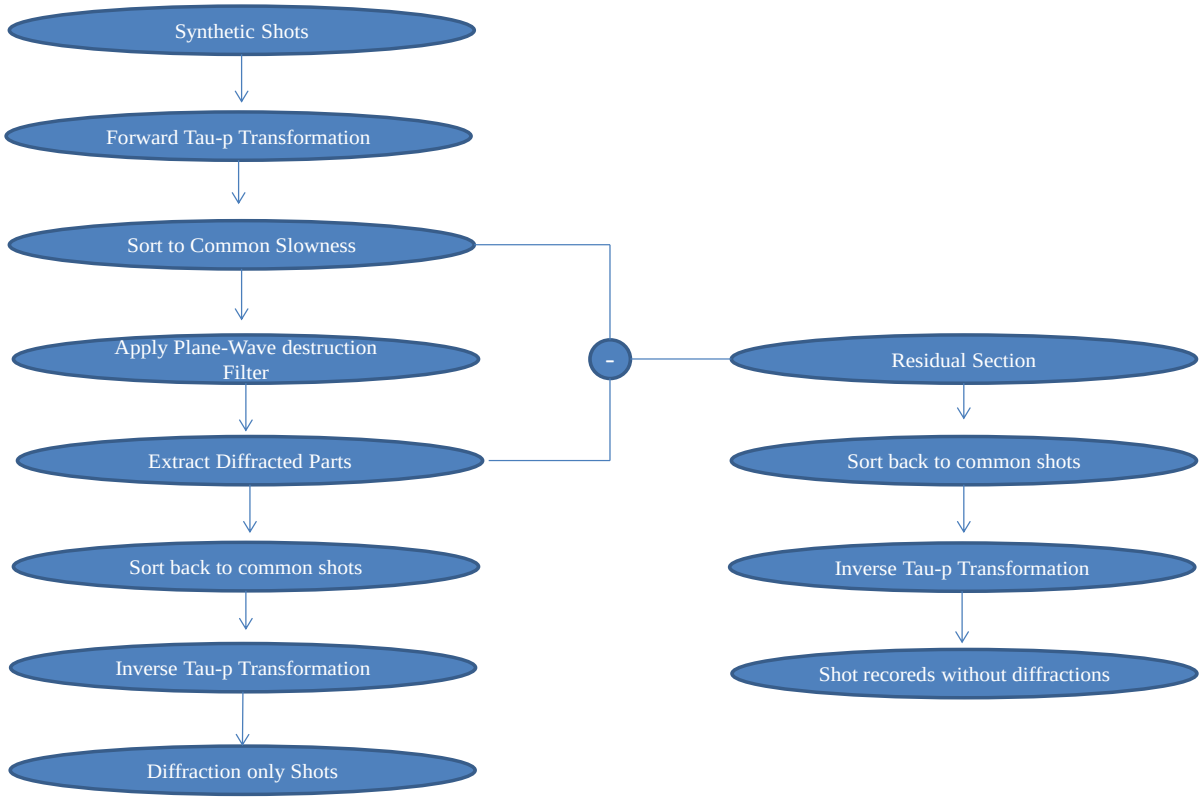

Figure 5.1: Flow diagram of the technique.

Minimum Slowness	-680 ms/km
Maximum Slowness	680 ms/km
Maximum time of interest	6000 ms
Minimum signed offset of interest	-11487 m
Maximum signed offset of interest	11487 m

Table 5.1: Parameters of Tau-p Transformation.

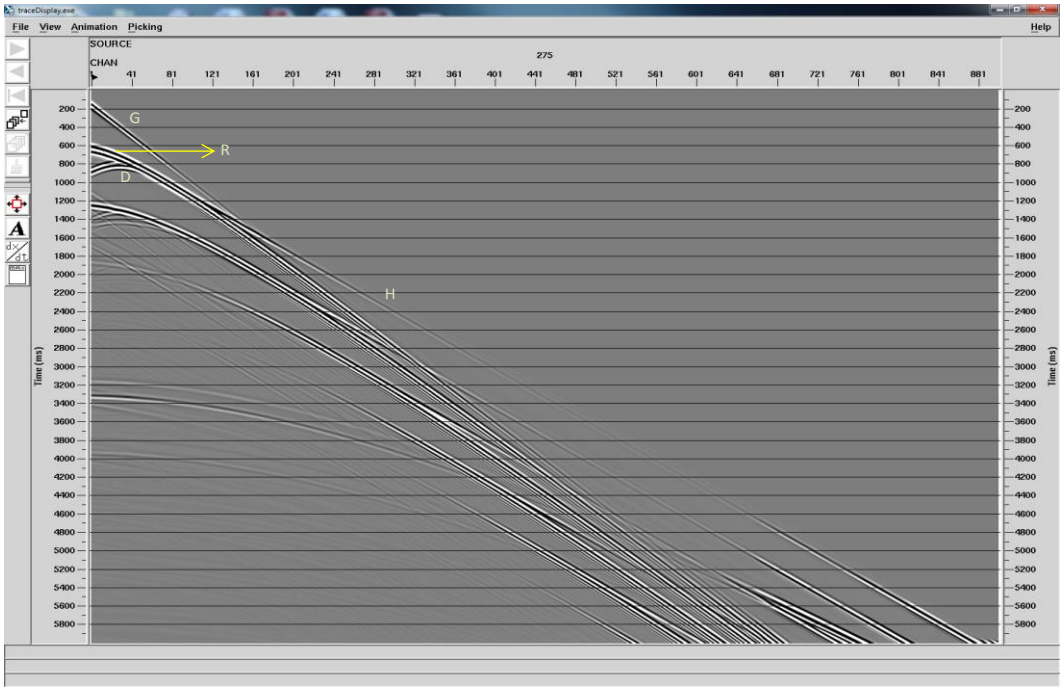

Figure 5.2: Source gather in (x-t) domain with direct wave G, primary reflection R, primary diffraction D and refraction H (Shot # 275).

Fig. 5.3 shows same shot point after tau-p transformation. This transformation is carried out by summing all traces in the space-time domain along a given range of slowness. In the case considered here we employed the range between -666 ms/km and 666 ms/km. The direct arrival G appears as a horizontal events after tau-p transformation instead of ideally a point. The reason is that its amplitude is very large at small traveltimes. As expected the reflection transform to an elliptical type of event R´. The primary diffraction transforms to a similar curve D´, since the primary reflection and diffraction in this case almost coincide in the space-time domain.

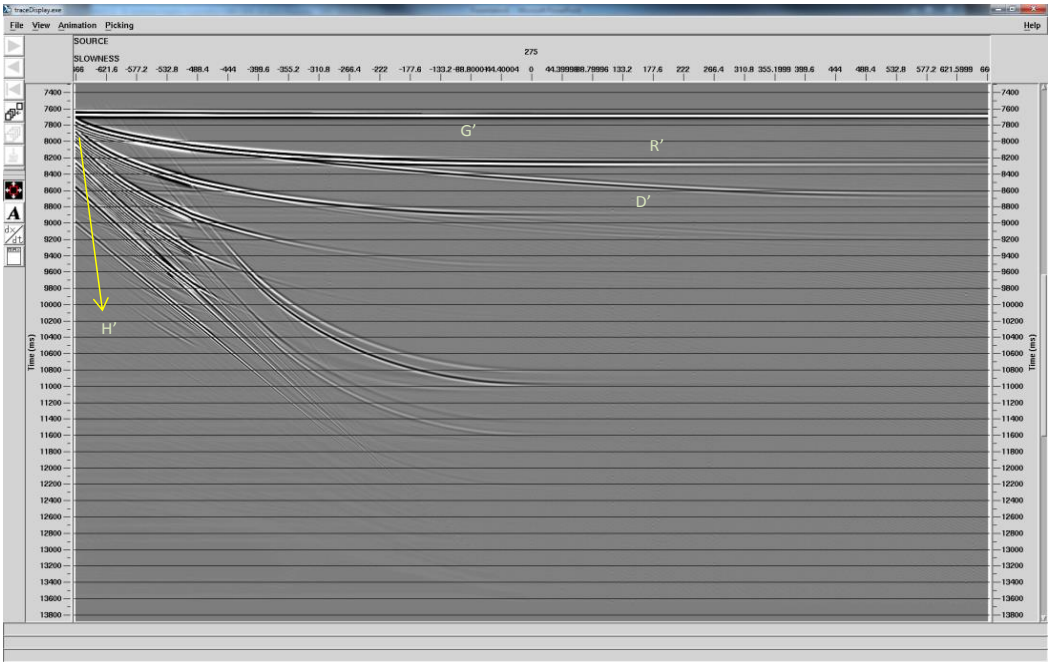

Figure 5.3: Tau-p transformation of shot gather in Fig. 5.2 (Shot # 275).

After all source gathers have been tau-p transformed, the next step is to form constant-*p* sections. Figure 5.4a shows an example of such a section for p = -16.68 ms/km. After a plane wave destruction filter has been applied to this constant-*p* section, the specular reflections have been removed and only diffractions and refractions are left as shown in Fig. 5.5.

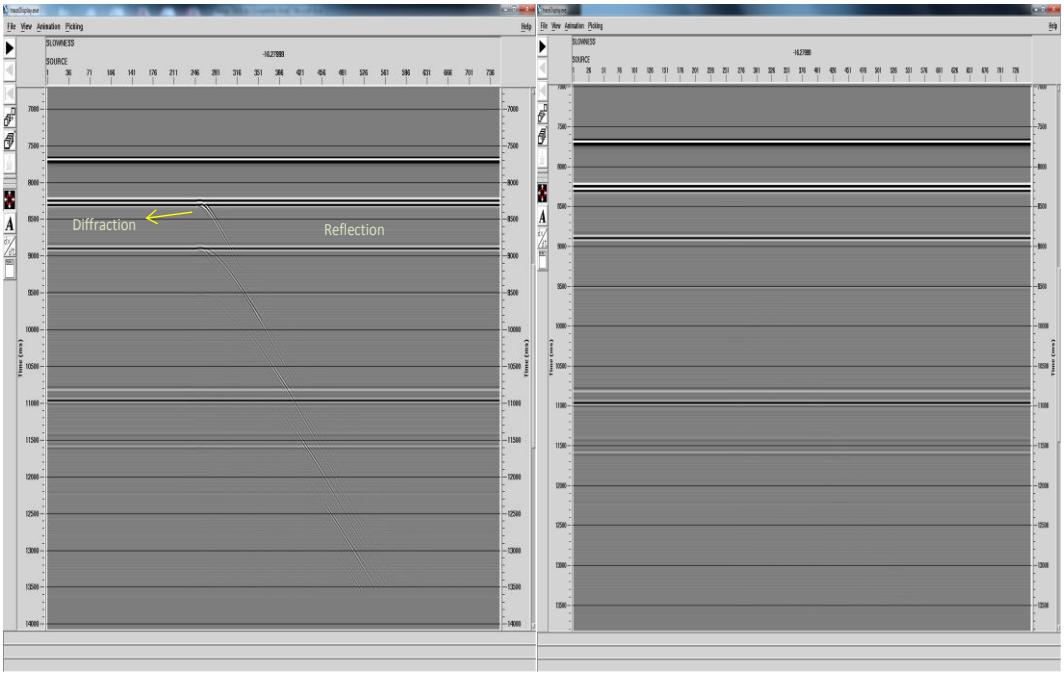

Figure 5.4: a) common slowness section of total wave field. b) same as (a) after subtraction (p= -16.27999).

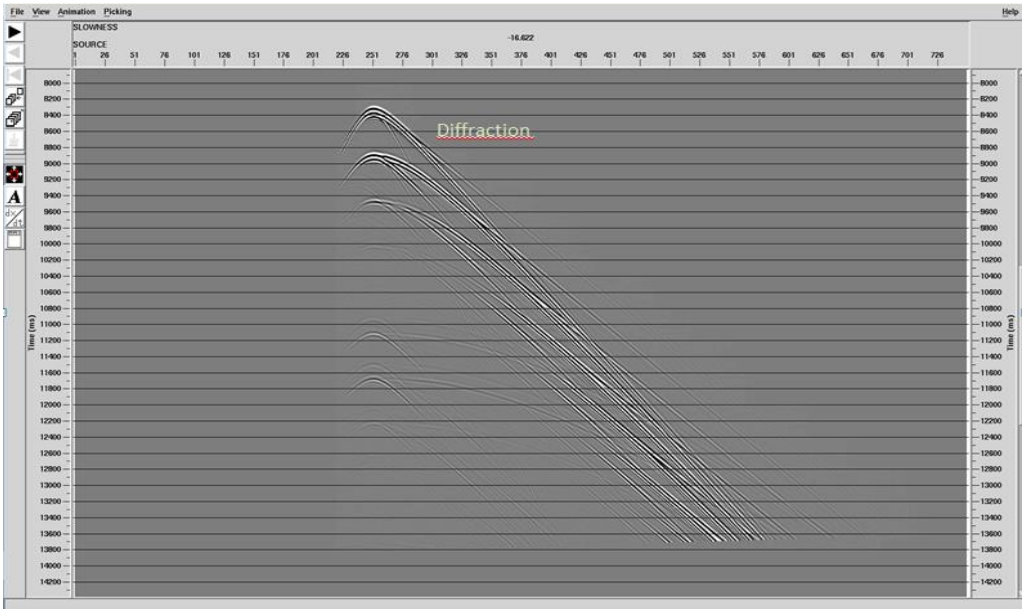

Figure 5.5: Common slowness section after removal of specular energy (P= -16.622).

Two different types of output can now be constructed. By collecting all the plane-wave destruction filtered constant-*p* sections like the one in Fig. 5.5 resorting back to tau-p gathers (cf. Fig. 5.6) and applying an inverse transform; a source gather without specular reflections can be obtained (cf. Fig. 5.7).

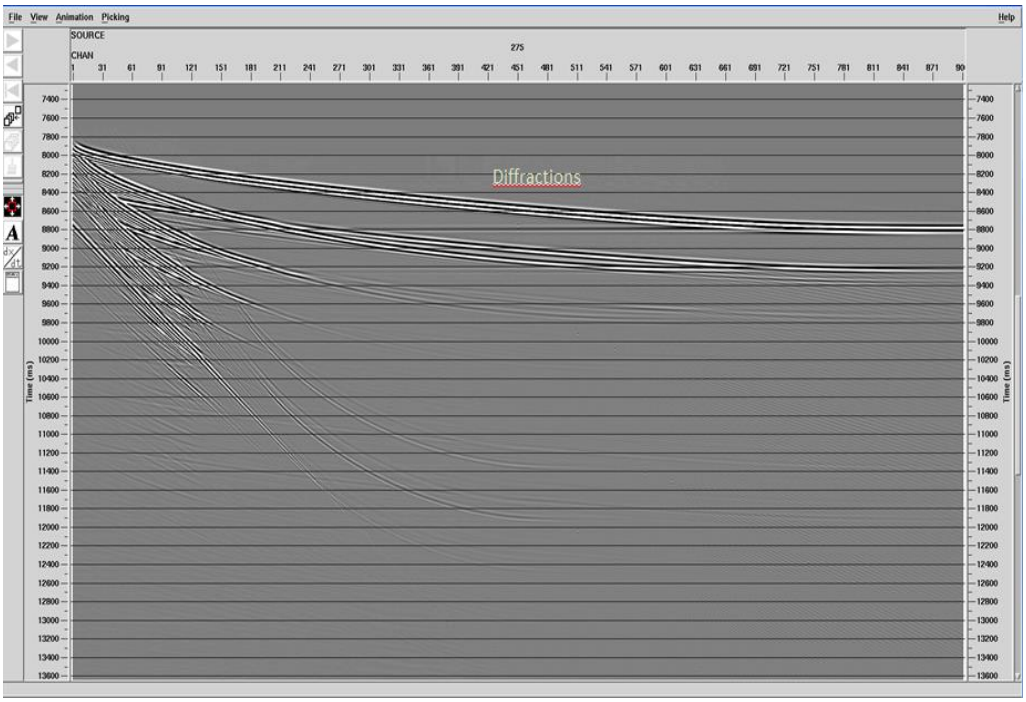

Figure 5.6: Sorting back diffractions into a tau-p gather.

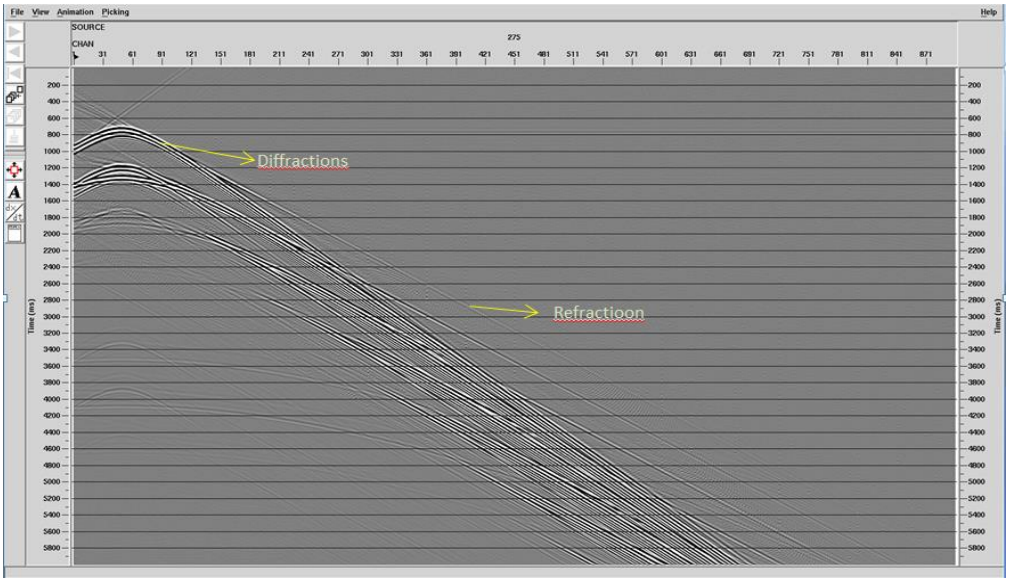

Figure 5.7: Inverse tau-p transformation of shot gather (shot # 275) with diffractions and refractions.

Alternatively, by sorting the diffraction subtracted common-p sections (cf. Fig. 5.4b) back into *p*- τ gathers and taking an inverse transform, source gather except diffractions can be obtained (cf. Fig. 5.8).

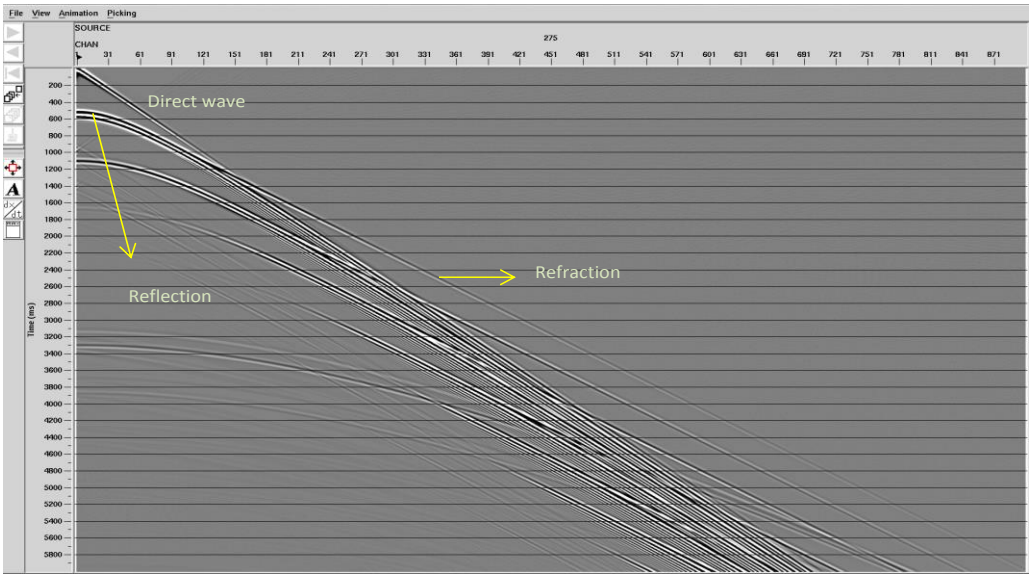

Figure 5.8: Shot point with diffractions removed.

5.2 PLANE-WAVE DESTRUCTION IN THE TAU-P DOMAIN (COMPLEX MODEL)

The same processing steps as described in section 5.1 have been repeated, but this time considering Model 2 (i.e complex model).

Figure 5.9 shows a source gather corresponding to shot # 400. Seismic events are labelled as direct wave (G), refraction from sea-floor (H), primary reflection from sea-floor (R) and primary diffraction (D).

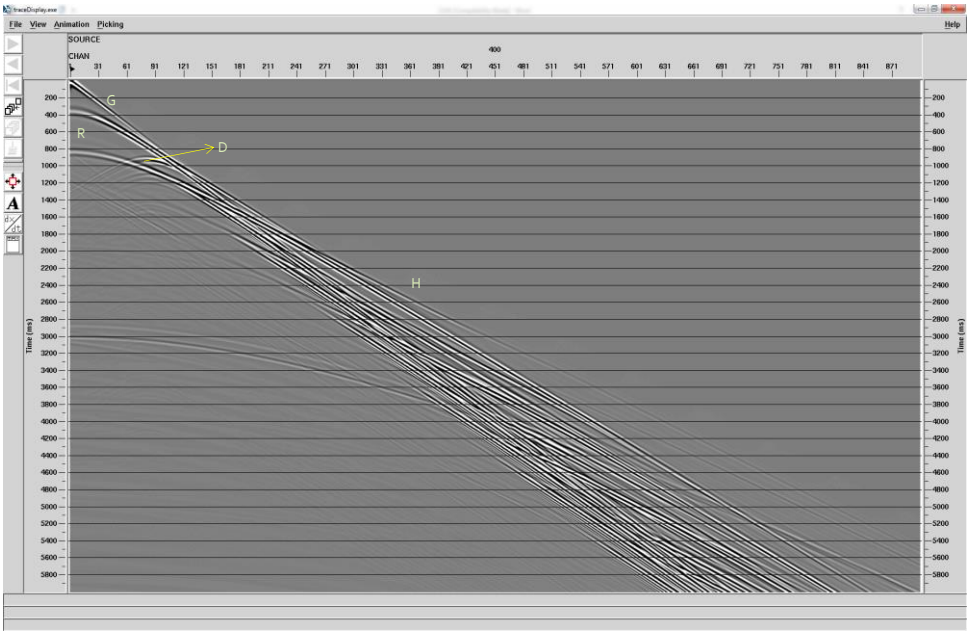

Figure 5.9: Source gather in (x-t) domain with direct wave G, primary reflection R, primary diffraction D and refraction H (Shot # 400).

Figure 5.10 shows the same shot record after tau-p transformation. The process is carried out by summing all the traces in the time-space domain along a range of slowness values (cf. Table 5.1). After tau-p transformation the primary reflection appears as an elliptical event R´. The direct wave G appears as a horizontal straight event G´ instead of point. The reason is that its amplitude is very high for small travel-time. Finally, the diffraction D appears to spread along an elliptical path and it partly coincides with the reflection in the time-space domain for this shot point. (cf. Fig. 5.10).

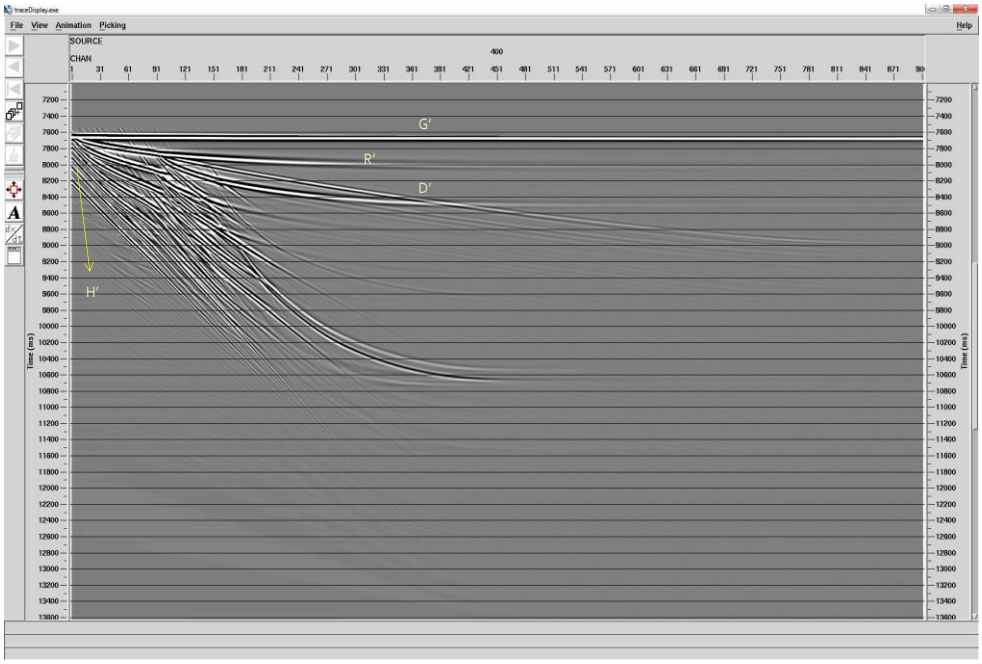

Figure 5.10: Tau-p transformation of shot gather in Fig. 5.9 (Shot # 400).

After all data has been transformed into the tau-p domain, the next step involves to form a constant-*p* section. Fig 5.11a shows a constant-*p* section for $p = -16.28$. Reflected events appear linear (at least locally), and application of a plane-wave destruction filter causes the removal of these specular reflections and corresponding enhancement of diffractions (cf. Fig. 5.11b).

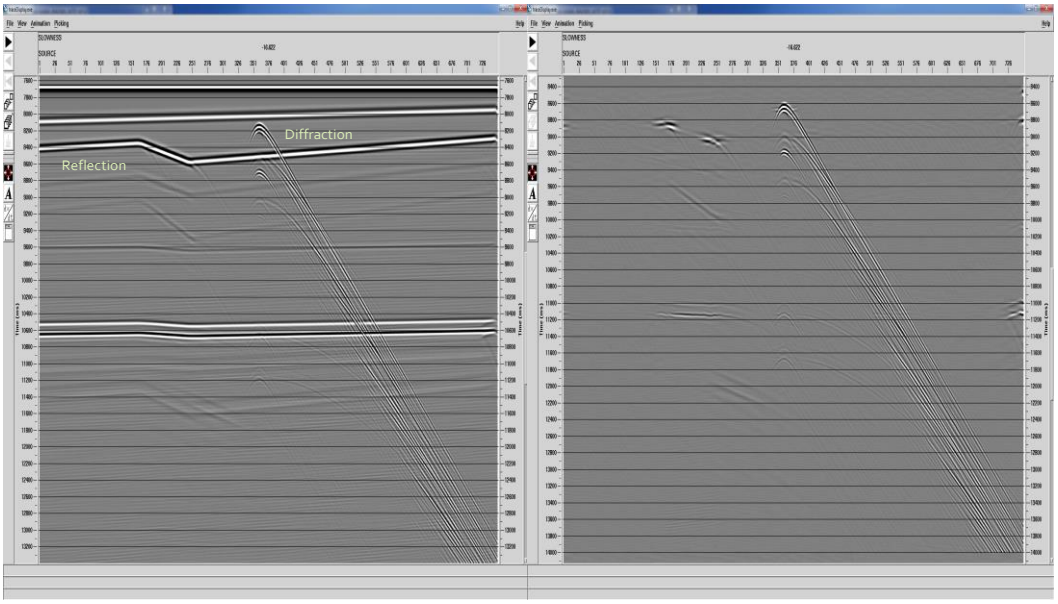

Figure 5.11: Common slowness section of total wave field before (a) and after subtraction (b) (p = -16.622).

The enhanced diffractions are sorted back into tau-p gathers (cf. Fig. 5.12) followed by an inverse tau-p transformation. In this way, a source gather without specular reflections is obtained (cf. Fig. 5.13).

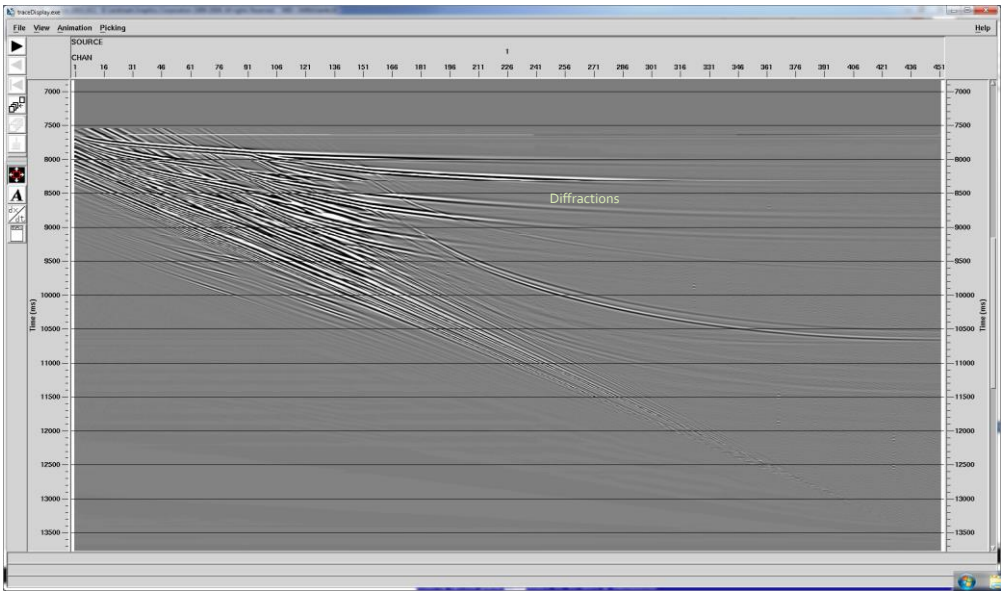

Figure 5.12: Sorting back diffraction into tau-p gathers.

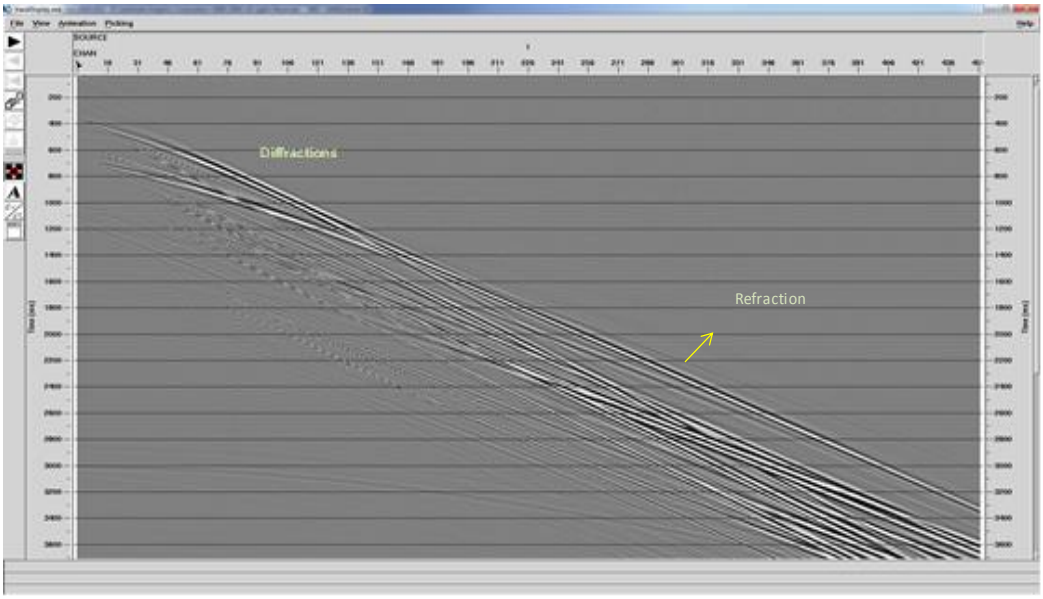

Figure 5.13: Shot record after Inverse tau-p transformation with diffractions and refractions.

Alternatively, by removing the diffraction enhanced contributions from the original data, a source gather is obtained containing all the seismic events except diffractions (cf. Fig. 5.14).

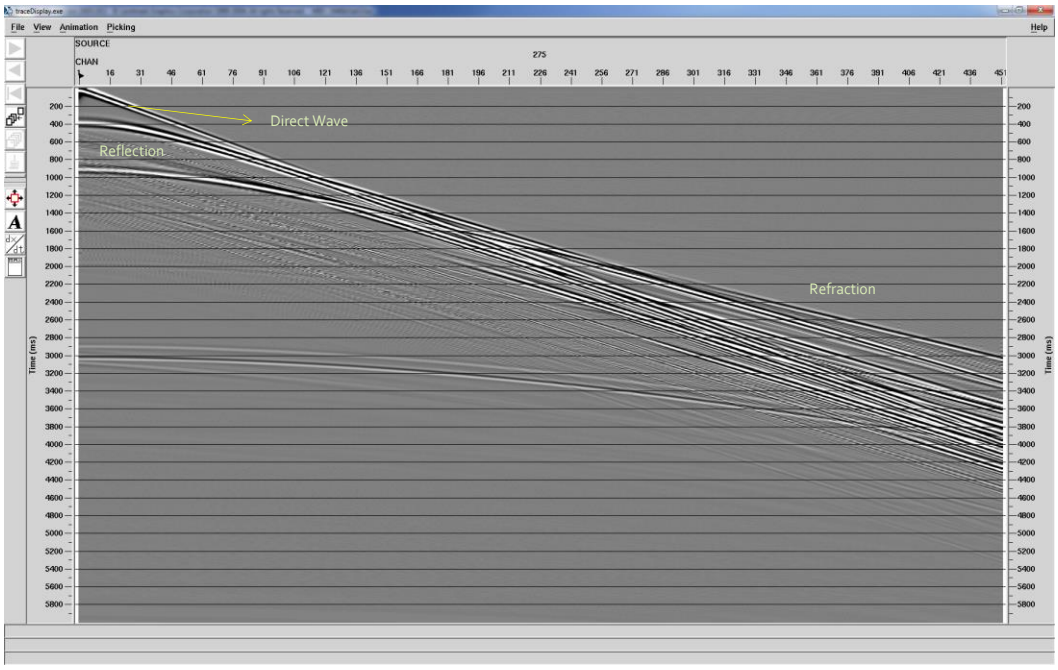

Figure 5.14: Common shot gather with no diffracted energy.

5.3 RESULTS USING THE MODIFIED CRS TECHNIQUE (SIMPLE MODEL)

5.3.1 ZO-SECTION ANALYSIS

The common reflection surface (CRS) technique is an extension to the classical common mid-point method to improve the signal to noise ratio. Conventional CRS method suppresses the diffracted events and enhances the reflected events along a generalized hyperbolic move-out. However diffracted events can be enhanced by using a modified version of the CRS technique.

Two steps are carried out for the CRS analysis:

- Average velocities are converted to root mean square velocities to calculate the parameter $C = 4/V_{rms}^2$ where V_{rms} is the root mean square velocity used to stack the approximated zero offset data.

- After data is stacked to an approximated zero offset (ZO) section the value of the parameter A is determined from Eq. (4.11) by scanning of a proper range of values in combination with a coherency criteria like semblance.

Figure 5.15 shows the approximated ZO (stacked) section which is used for the CRS analysis.

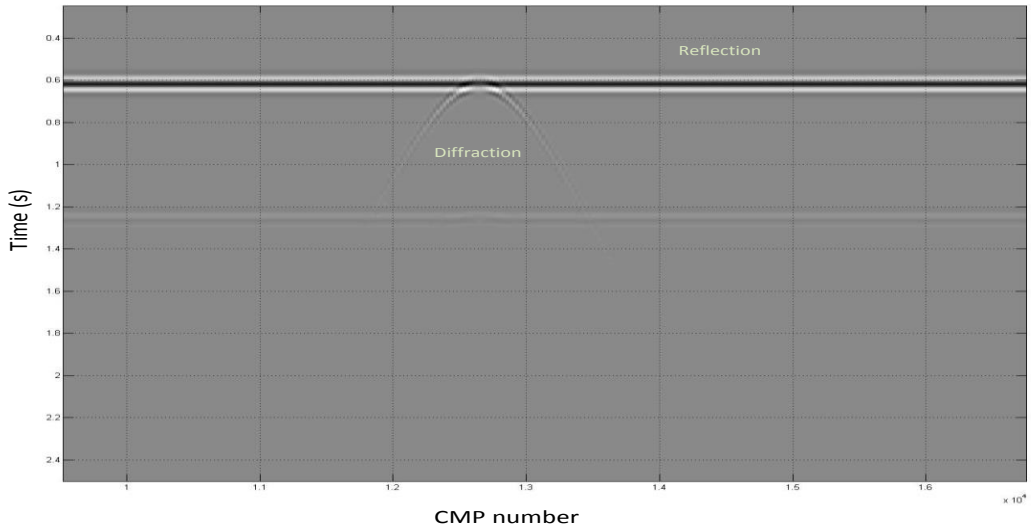

Figure 5.15: Approximated ZO (stacked) section.

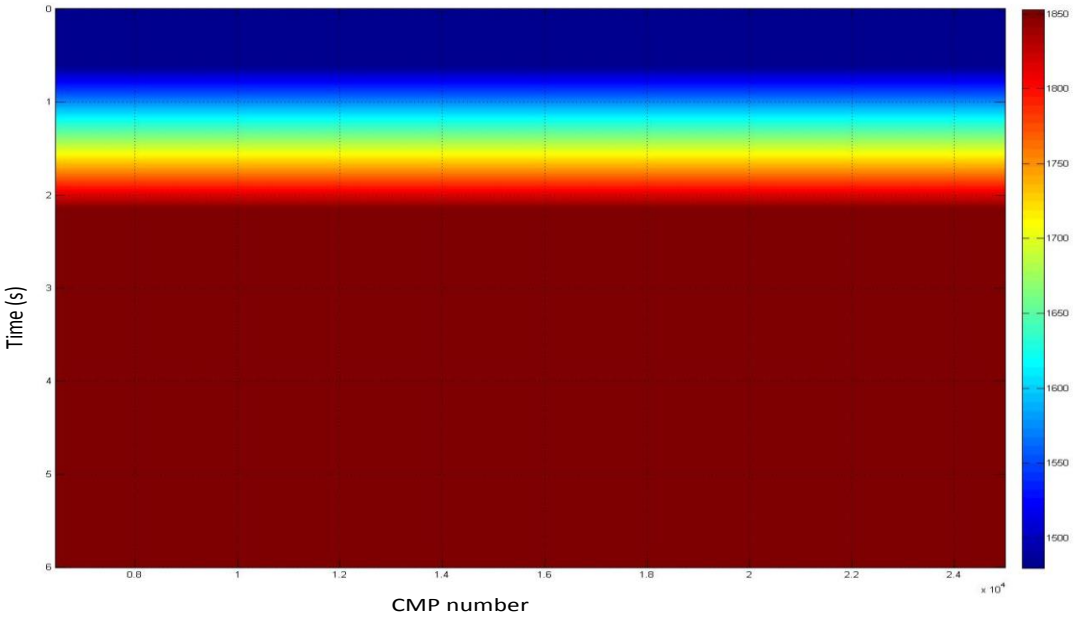

Figure 5.16: V_{rms} velocity map of stacked section.

In case of diffraction enhancement using the modified CRS method, only two parameters are required namely A and C. Fig (5.16) shows the map of C values while Figure 5.17 shows the coherency map of parameter A based on semblance. We can see that the primary

diffraction is characterized by high coherency values both at its apex and towards the flanks. However, in case of diffracted multiples the values are in general lower and also shifted more to the deeper parts of the flanks. The reason is that these multiples propagate in the water, but in the CRS analysis the parameter C is set to values of the true earth model.

Figure 5.18 shows the enhanced-diffraction result obtained employing this technique. The primary diffraction has been well resolved, but separation noise does exist. This latter issue can probably be reduced if a more accurate multi-parameter analysis was carried out for A and C. The area marked with the circles in order to unravel possible multiples.

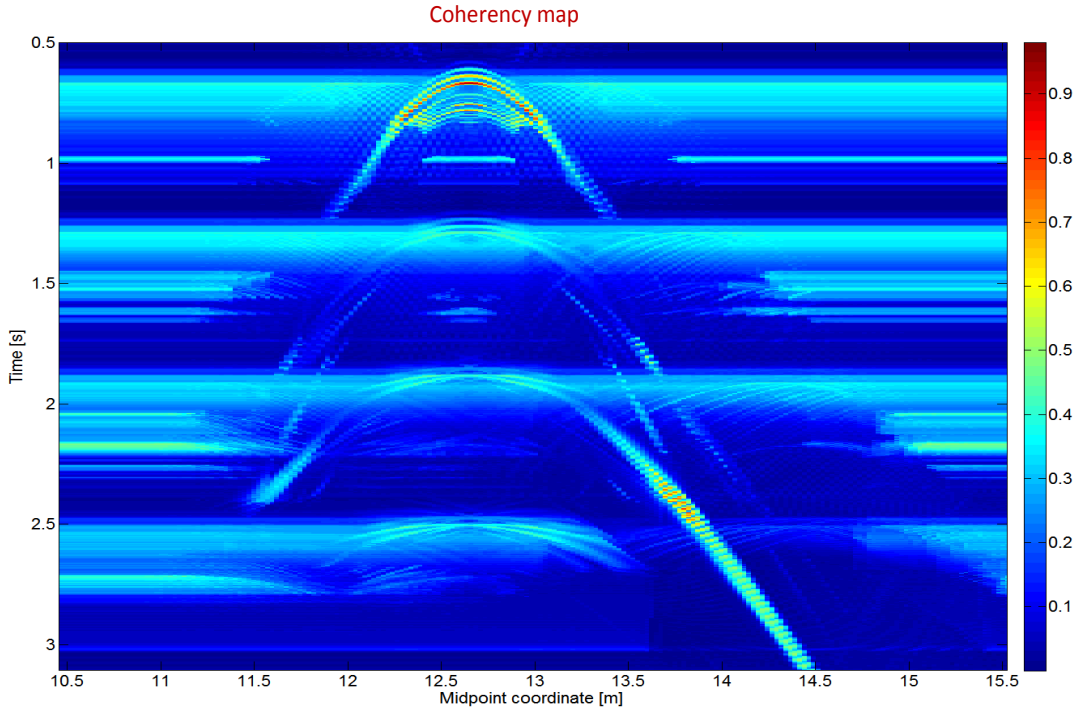

Figure 5.17: The coherency map of parameter A based on Semblance.

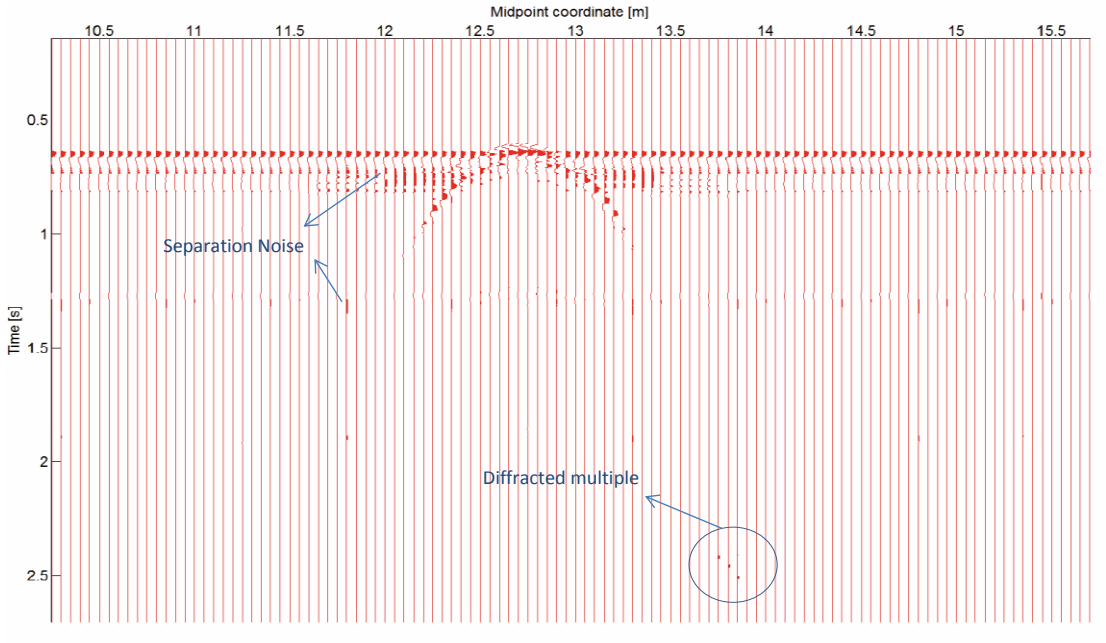

Figure 5.18: A zero-offset CRS-diffraction stack section based on parameter A and C.

The same procedure was then repeated, but this time employing the water velocity (1480 m/s) for the whole model (i.e. C parameter). Figure 5.19 shows again the semblance plot for parameter A, and this time high coherency values are associated for both the primary diffractions and corresponding multiples as expected.

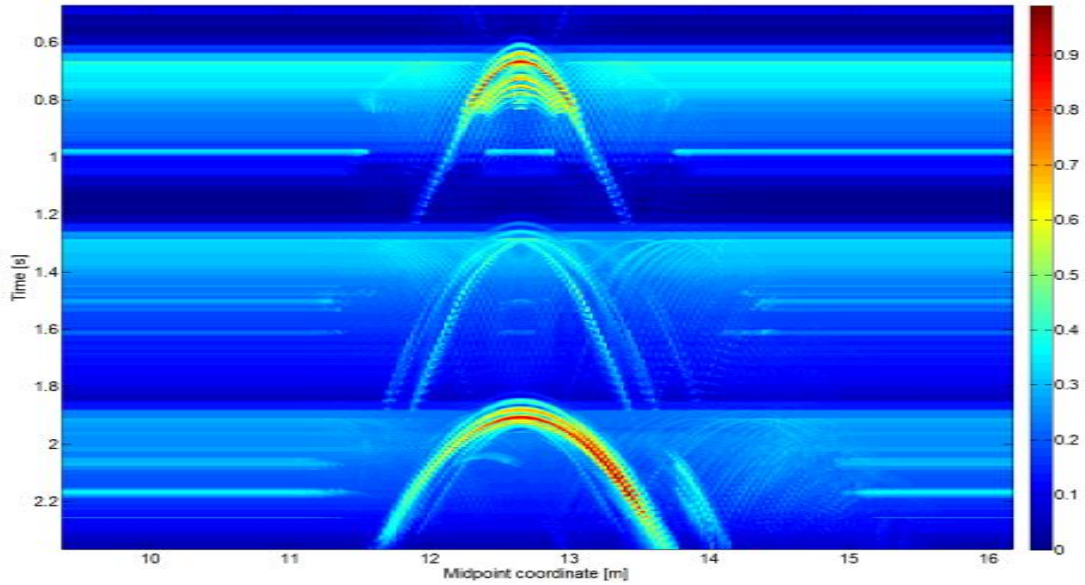

Fig. 5.19: The coherency map of parameter A based on Semblance using water velocity 1480 m/s for C paramter

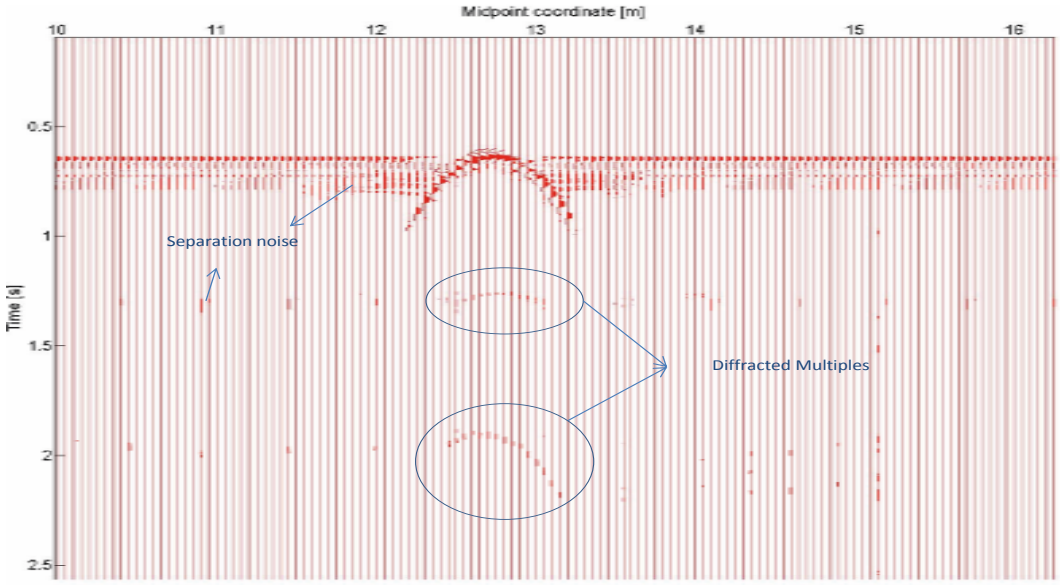

Figure 5.20: A zero-offset CRS-diffraction stack based on paramter A and water velocity.

The corresponding diffraction-enhanced stack is shown in Fig. 5.20. As before, some separation noise does exist due to lack of fine tuning of parameter A and C. The area marked by circles in Fig. 5.20 show diffracted multiples which are recovered well.

5.4 RESULTS USING THE MODIFIED CRS TECHNIQUE (COMPLEX MODEL)

5.4.1 ZO-SECTION ANALYSIS

The same procedure was applied using the modified version of CRS but this time employing the complex data. The interval velocities in time were converted to RMS velocities to generate a ZO (stacked) section. Figure 5.21 shows the approximated ZO (stacked) section used for the CRS analysis.

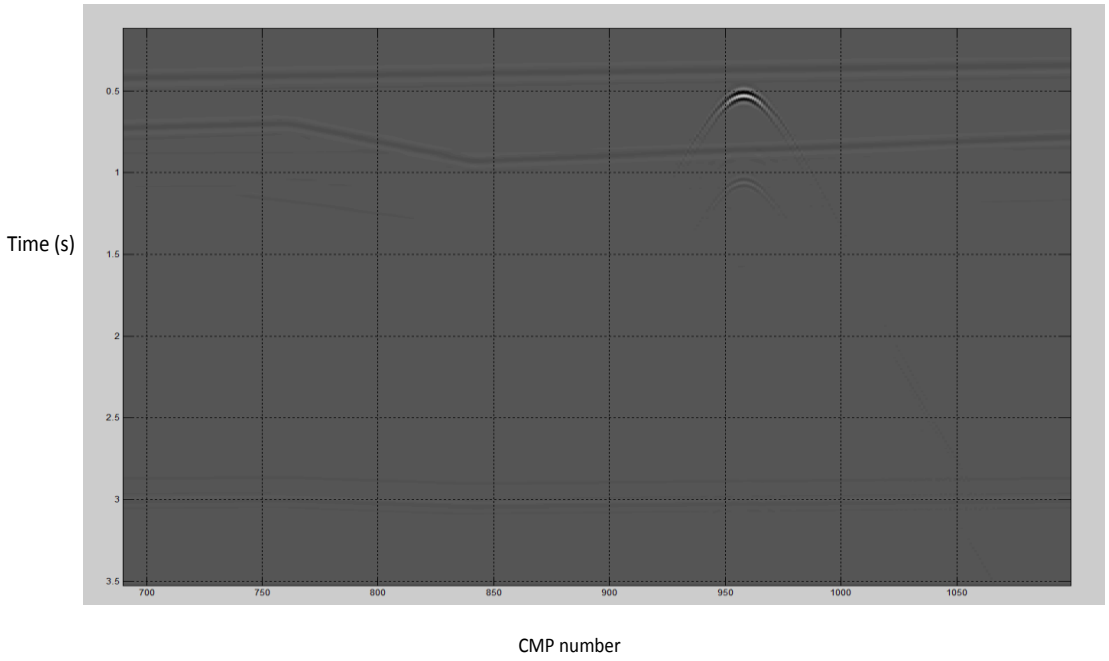

Figure 5.21: Approximated ZO (stacked) section.

As before, the values of C are calculated by using $C = 4/V_{rms}^2$. Figure 5.22 shows the map of C values. Correspondingly, the coherency map of parameter A is shown in Fig. 5.23. As expected, the primary diffraction is defined by high coherency, but somewhat more mixed for the multiples.

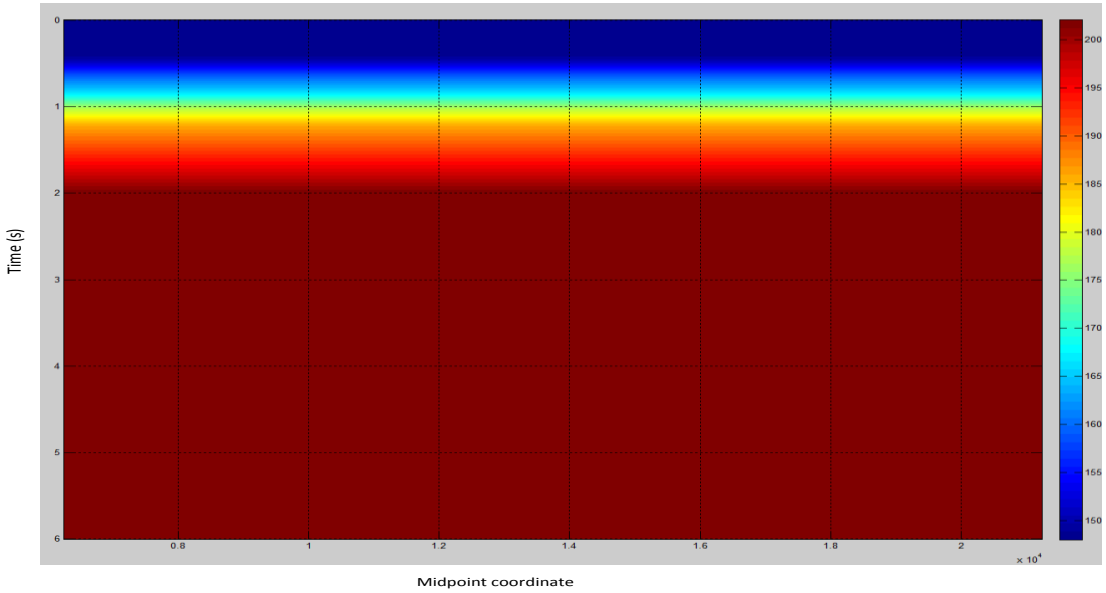

Figure 5.22: V_{RMS} velocity map of stacked section.

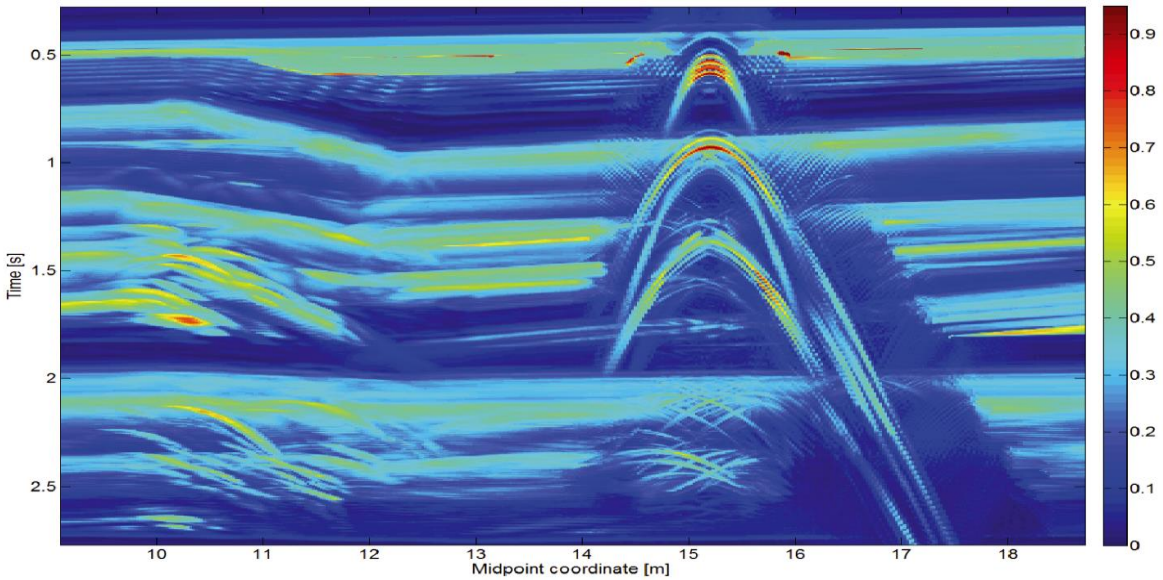

Figure 5.23: The coherency map of parameter A based on Semblance.

Figure 5.24 shows the diffraction enhanced stack. The primary diffraction is well recovered and also the separation noise is less than in the case of simple model. The reason is that the diffraction no longer coincide with the sea reflector. By considing the circled area shown in Fig. 5.24, the first diffracted multiple is seen to be fairly well recovered and smaller part of flanks.

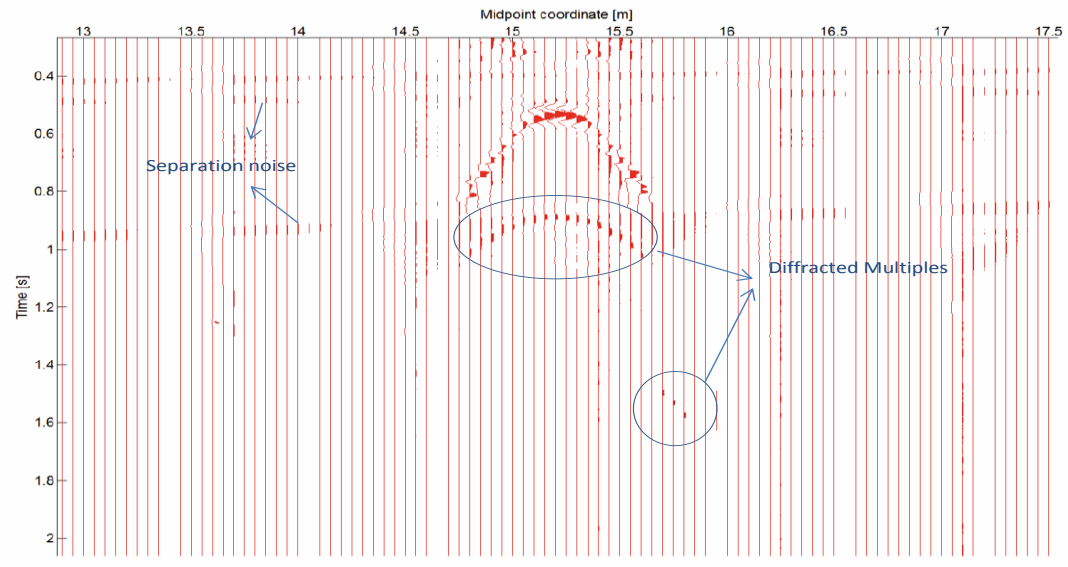

Figure 5.24: A zero-offset CRS-diffraction stack section based on parameter A and C (complex model).

CHAPTER 6 DISCUSSION AND CONCLUSION

The main objective of this thesis has been to investigate possible techniques for both enhancing and removal of diffractions and their associated water bottom multiples.

We have investigated two different techniques: i) Plane wave destruction in the tau-p domain and ii) modified version of CRS. Two controlled datasets were generated using FD modelling. One was a simple model which includes one reflector only and a point diffractor while the other consisted of a dipping reflector, a point diffractor and a dipping reflector along a fault. First data were sorted into different domains to see how diffractions and reflections behave. Sorting to CO sections showed the best separation.

Based on this observation we used Plane wave destruction filtering in the tau-p domain method to separate reflections and diffractions. After sorting to constant-*p* sections, diffractions appear as hyperbola and reflections appear as locally continuous straight events. Thus such sections naturally separate reflections and diffractions and further by using plane wave destruction filtering, specular reflections can be easily eliminated. This technique was found to work well both in enhancing and removing diffractions for both simple and complex data.

The other technique investigated in this thesis was modified CRS method. It worked quite well for both models, when it comes to enhancement of the primary diffraction. However, in case of the diffracted multiples, care has to be taken when it comes to parameter C. Since the multiples in question are formed in the water column, better results can be obtained by using the water velocity as input to the C calculation. However for deep scatterers this will not be sufficient. Since CRS is a kinematic method, amplitudes are not preserved. Thus removal implies use of adaptive techniques.

REFERENCES

ASGEDOM, E. G., GELIUS, L.-J., AUSTENG, A. & TYGEL, M. 2011 b. A new approach to post-stack diffraction separation. SEG Expanded Abstract 30. Society of Exploration Geophysicists.

ASGEDOM, E. G., GELIUS, L.-J. & TYGEL, M. 2011 a. Diffraction Separation Using the CRS Technique: A Field Data Application. 12th International Congress of the Brazilian Geophysical Society.

ASGEDOM, E. G., GELIUS, L. J. & TYGEL, M. 2011 c. Higher-resolution determination of zero-offset common-reflection-surface stack parameters. *International Journal of Geophysics*.

DELL, S. & GAJEWSKI, D. 2011. Common-reflection-surface-based workflow for diffraction imaging. *Geophysics,* 76**,** S187-S195.

DURRANI, T. & BISSET, D. 1984. The Radon transform and its properties. *Geophysics,* 49**,** 1180-1187.

ELBOTH, T. 2010. *Noise in Marine Seismic Data.* degree of Philosophiae Doctor, University of Oslo.

ELBOTH, T., GEOTEAM, F. & HERMANSEN, D. 2009 a. Attenuation of noise in marine seismic data. SEG Technical Program Expanded Abstracts. 3312-3316.

ELBOTH, T., REIF, B. A. & ANDREASSEN, Ø. 2009. Flow and swell noise in marine seismic data. *Geophysics,* 74**,** Q17-Q25.

FACCIPIERI, J. H., SERRANO, D. R., GELIUS, L.-J. & TYGEL, M. 2013. Recovering diffractions in CRS stacked sections. *First Break,* 31**,** 27-31.

FOMEL, S. 2002. Applications of plane-wave destruction filters. *Geophysics,* 67**,** 1946-1960.

FOMEL, S., LANDA, E. & TANER, M. T. 2007. Poststack velocity analysis by separation and imaging of seismic diffractions. *Geophysics,* 72**,** U89-U94.

GELIUS, L.-J. & JOHANSEN, T. A. 2010. *Petroleum Geophysics. UniGEO AS, Bergen*.

GRUDE, S., OSDAL, B. & LANDRØ, M. 2013. Sea- bed diffractions and their impact on 4D seismic data. *Geophysical Prospecting,* 61**,** 199-214.

JÄGER, R., MANN, J., HÖCHT, G. & HUBRAL, P. 2001. Common-reflection-surface stack: Image and attributes. *Geophysics,* 66**,** 97-109.

KEAREY, P., BROOKES, M. & HILL, I. 2002. An introduction to geophysical exploration Third Edition ed.: Wiley Blackwell Science, West Sussex (ISBN: 978-0-63204-929-5).

KHAIDUKOV, V., LANDA, E. & MOSER, T. J. 2004. Diffraction imaging by focusing-defocusing: An outlook on seismic superresolution. *Geophysics,* 69**,** 1478-1490.

LANDA, E. & KEYDAR, S. 1998. Seismic monitoring of diffraction images for detection of local heterogeneities. *Geophysics,* 63**,** 1093-1100.

MANN, J., SCHLEICHER, J. & HERTWECK, T. 2007. CRS Stacking–A Simplified Explanation. 69th EAGE Conference & Exhibition.

MOSER, T. & HOWARD, C. 2008. Diffraction imaging in depth. *Geophysical Prospecting,* 56**,** 627-641.

OLHOVICH, V. 1964. The causes of noise in seismic reflection and refraction work. *Geophysics,* 29**,** 1015-1030.

STEIN, S. & WYSESSION, M. 2003. *An introduction to seismology, earthquakes, and earth structure,* Willy-Blackwell.

STORBAKK, S. 2012. *De-noising of marine seismic data.* Master program in geosciences, University of Oslo.

TANER, M. T. & FOMEL, S. 2006. Separation and imaging of seismic diffractions using plane-wave decomposition. 2006 SEG Annual Meeting, Society of Exploration Geophysicists, 2401-2404.

TATHAM, R. H., KEENEY, J. W. & NOPONEN, I. 1983. Application of the tau-p transform (slant-stack) in processing seismic reflection data*. *Exploration Geophysics,* 14**,** 163-172.

TRAVIS, T. & WOODBURN, N. 2010. Processing challenges from Arctic latitude: attenuation of diffraction multiples from ice-sourcing tracks.

YILMAZ, Ö. 2001. *Seismic Data Analysis,* Society of Exploration Geophysicists

Fugro internal notes, 2012.

Promax Manual, 2012.

www.unigeo.no